The reniform superposition compound eyes of *Nephrops norvegicus*: Optics, susceptibility to light induced damage, electrophysiology and a ray tracing model.

Edward Gaten[1], Steve Moss[2] and Magnus Johnson[3]

1 Biology Department, University of Leicester, University Rd, Leicester, LE1 7RH

2 Department of Biology, University of Hull, Hull, HU6 7RX

3 Centre for Environmental and Marine Sciences, University of Hull, Scarborough, YO11 3AZ

Abstract

The large reniform eyes of the reptant, tube-dwelling decapod *Nephrops norvegicus* are described in some detail. Optically these reflecting superposition compound eyes are a little unusual in that they are laterally flattened, a feature that may enhance their sensitivity in that region, albeit at the expense of resolution. Electrophysiological and anatomical investigations suggest that the eyes are able to tune to appropriate spectral and temporal sensitivities in the long and short term through movement of proximal pigments and possibly rhabdom adaptation. Although exposure to ambient surface light intensities is shown to cause damage to the retinal layer, especially in deeper living animals, there is no evidence yet that demonstrates an impact of eye damage on their survival. It is suggested that experimentation on marine decapods, with sensitive eyes, requires that particular attention is paid to their visual sensitivity.

Introduction

All large crustaceans have compound eyes. The apposition type is the simplest form of such eyes and is common in all primitive Crustacea and some brachyuran crabs, amphipods and isopods. In this type of eye, each photoreceptive rhabdom has a single aperture through which light enters such that the scene that the animal observes is simply a matrix of “pixels”, one for each facet (Figure 1a). Resolution at the level of individual receptors in this case is determined by the angular separation of the ommatidia. Generally, these eyes are limited in low light conditions by the small aperture through which light passes to reach the rhabdom (Land & Nilsson, 2002). In compound eyes different solutions have appeared which serve to increase the absolute sensitivity of the eye. They all use superposition optics, in which light from one direction is focussed onto the target rhabdom via a large number of

facets, resulting in an increase in sensitivity of up to three orders of magnitude (Figure 1b). Refracting superposition optics are used in various crustacean taxa whilst parabolic superposition optics have been described in some hermit crabs and swimming crabs (Nilsson, 1989). However, the majority of decapod crustaceans have reflecting superposition eyes which can easily be identified by the fact that they have square corneal facets arranged in a lattice and a distinct clear zone between the phororeceptive rhabdom layer and the dioptric layer (Land, 1976, Gaten, 1998).

The large eyes of *Nephrops norvegicus* are arguably the most recognisable feature of the animal, resulting in its generic name, derived from the Greek *nephros* (kidney) and *ops* (eye). The eyes of *Nephrops* have attracted the attention of researchers because of their size which facilitates anatomical and physiological investigations and, in Europe, their ease of availability as they are a commercially targeted species.

Light intensity is important with respect to the ecology, behaviour and prosecution of this species. However, as these aspects are covered fully in this volume elsewhere we will concentrate on physiological and anatomical aspects of *Nephrops* vision.

Eye structure

The eye of *Nephrops norvegicus* has been described in detail (Aréchiga & Atkinson, 1975; Loew, 1976); the following account is a brief description of this large and unusual reflecting superposition eye. The eye is one of the largest of all crustacean eyes (Figure 2), measuring up to 10 mm along the antero-posterior axis, and it is borne on a short moveable eyestalk. The eye is quite unusual among decapods with superposition optics in its lack of spherical symmetry; the distinctive kidney shaped eye being oval when viewed from the lateral aspect. More than 10,000 ommatidia are present in the eye with around 3,000 of these displaying eyeshine in the dark-adapted eye (Figure 3a). The corneal facets are square except for a small region close to the dorsal margin of the eye which consists of hexagonal facets. This was formerly described as a growth zone where newly-formed hexagonally-packed ommatidia develop and mature (Parker, 1890; Shelton *et al*., 1981). However, this region uses

apposition optics and more likely has a special function in relation to viewing the brighter downwelling light (Tokarski & Hafner, 1984; Gaten, 1994).

Sections through the eye reveal distal crystalline cone cell and proximal retinula cell layers, separated by a clear zone (Figure 3b). In longitudinal sections of the eye, the longest ommatidia are anterior and posterior, some 20% longer than those from the centre of the eye (Figure 3b). The lengths of the ommatidia increase from dorsal to ventral (Figure 3c).

The ommatidial structure is typical of a reflecting superposition eye (ref), consisting of a distal dioptric apparatus (for focusing the light) and a proximal retinula cell layer (where the image is formed). Distally, square corneal facets, up to 60μm across, are secreted by two corneagenous cells. Underlying the facet there are four cone cells that secrete a central crystalline cone. Proximally four cone cell processes cross the clear zone as a quadripartite cone stalk (or crystalline tract). The cones are separated by distal pigment cells which contain both reflecting pigment and dark shielding pigment (Figure 3d). In phase contrast micrographs of longitudinal sections the distal shielding pigment can be seen surrounding the middle 2/3 of the cone (Figure 3e). The reflecting pigment is birefringent and is revealed by using crossed polaroid filters. It extends approximately 1/2 the length of the cones (Figure 3f). The reflecting pigment granules are arranged in the form of a reflecting multilayer (Land, 1972) surrounding the sides of each cone and can be seen in transverse sections of the cones (Figure 3d). The distal pigment cells do not extend beyond the proximal end of the cone, except in light-damaged eyes (Gaten, 1988) and neither these cells nor the pigment granules move in response to light (Shelton *et al*, 1986).

There are eight retinula cells in each ommatidium and each retinula cell contributes microvilli to a central, light-sensitive spindle-shaped rhabdom (Figure 4a). In cross-section, the distal part of the rhabdom is surrounded by the four lobes of retinula cell 8, each contributing a rhabdomere to the small distal rhabdom (Figure 4c). The lobes of R8 are in turn surrounded by the cell bodies of retinula cells 1 to 7 (Figure 4c). The cone stalk separates to form four separate cone cell processes (Figure 4b) each of which lies at one corner of the rhabdom (Figure 4c). The majority of the spindle-shaped

rhabdom is formed by the remaining retinula cells (R1-7). The proximal rhabdom appears banded due to the alternating layers of orthogonally orientated microvilli (Figure 4d). The retinula cell nuclei are located just distal to the rhabdoms. Below the rhabdoms, the retinula cells form axons that extend proximally through the basement membrane to the first optic neuropil.

A tapetum is present behind the rhabdoms. It is formed by reflecting pigment cells each of which extends over several ommatidia. The reflecting pigment granules are spherical, about 0.4 μm in diameter and densely packed within the tapetal cells (Figure 4e). The basement membrane is formed of a layered collagenous sheet with the retinula cell axons passing through regularly spaced holes (Figure 4f).

Light-induced migration of retinula cell screening pigments has been observed in most decapod species (Kleinholz, 1961; Land, 1981; Parker, 1932). Some migration of proximal shielding pigment occurs in response to light in *N. norvegicus*, although the distal shielding pigment and the reflecting pigment do not migrate during light adaptation (Shelton *et al*, 1986). Shielding pigment granules are present in the retinula cells, with the numbers of granules being related to the depth at which the animals are caught (Gaten *et al*., 1990). The pigment is present close to the basement membrane in dark-adapted eyes (Figure 5a) and it migrates distally to shield the rhabdom during light adaptation (Shelton *et al*., 1986). The extent and speed of the migration is independent of the light levels although the normal fully dark- and light-adapted positions also vary with the habitat depth (Gaten *et al*., 1990).

Eye development

In *Nephrops norvegicus* eggs are laid in the autumn and attached to the pleopods (Eriksson et al, this volume) where they remain throughout development (Farmer, 1975). After the first few divisions, development may be arrested for up to seven months. After recommencement of development in the spring, the embryos mature rapidly. There are usually two or three planktotrophic zoeal stages

Although they can generally be regarded as apposition in the larval animals (Figure 5b) at any stage in the embryonic development of the eye of *N. norvegicus* a gradient of increasing ommatidial maturity can be seen from posterior to anterior (Figure 6a) so the temporal sequence of developmental stages can therefore be displayed spatially in a longitudinal section of the eye. The monolayer of epidermal cells merges into eye tissue at the posterior margin of the eye. As the depth of the retina increases, each cell becomes elongated and appears to extend from the cornea to the basement membrane (Figure 6b).

The next region, moving anteriorly, is where cell differentiation occurs. Distal invaginations are seen occasionally in the region where clusters of retinula cells sink away from the cornea (Figure 6c). The retinula cell clusters change shape during development , with cross-sections of the early retinula cell clusters show that initially they are arranged in a square pattern (Figure 6d). The eighth retinula cell is always positioned posterior to the other seven cells. The latter are arranged in three rows of cells. These cells become progressively wedge-shaped, eventually meeting centrally (Figure 6e). In the most mature ommatidia rudimentary microvilli can be seen interdigitating in the centre of the cluster to form a presumptive rhabdom.

As the retinula cells move proximally, clusters of cone cells and corneagenous cells are found below the cornea. By the time clear ommatidia are recognizable, the cone cells have also sunk away from the cornea (Figure 6f). However, the distal extension of the cone cells always retains contact with the cornea between the corneagenous cells.

In the most anterior ommatidia of the mature embryo the cone and corneagenous cells are arranged as in the first zoea. The unpigmented cone cell layer and the heavily pigmented rhabdom layer each occupy half of the length of the ommatidia. Some shielding pigment can be seen in the retinula cells and occasional strings of larger pigment granules are present between the retinula cells. Groups of eight axons can be seen passing through the basement membrane.

Embryonic development of the eyes of *N. norvegicus* closely follows the pattern seen in lobster *Homarus americanus* (Hafner & Tokarski, 2001) and crayfish *Procambarus clarkia* (Hafner & Tokarski,

1998). Harzsch & Hafner (2006) concluded that a conserved ontogenetic process of retinal development in the Tetraconata was supported by the similarities observed in several crustacean species.

The eye of the 1st zoea (Figure 7a) is a typical larval apposition eye with the cone closely apposed to the thin rhabdom. It is similar to those found in other larval crustaceans (Nilsson, 1983). The cornea consists of circular biconvex facets, arranged hexagonally. In each ommatidium two corneagenous cells and four cone cells are grouped together in an inverted cone shape beneath the facet (Figure 7a). There is no crystalline material contained within the cone cells. The proximal ends of the cone cells abut the distal end of the rhabdom.

The area between the cones contains the retinula cell nuclei, although the retinula cell cytoplasm is mostly within the rhabdom layer. Proximal shielding pigment is distributed throughout the retinula cells and is visible alongside the rhabdoms (Figure 7b). The top of the rhabdom layer is marked by an extensive pigment shield consisting of larger pigment grains than those found between the rhabdoms (Figure 5B). A layer of reflecting pigment cells is also found here, overlaying the shielding pigment. The processes of these reflecting pigment cells extend proximally between the rhabdoms.

The rhabdoms are thin, cylindrical and extend almost down to the basement membrane. They are formed by the interlocking rhabdomeres of seven retinula cells over most of their length (R1 to R7). The main rhabdoms have a banded appearance due to the orthogonal layering of the microvilli (Figure 7c). At the distal end of the rhabdom, R8 contributes a small rhabdomere in which no layering is seen (Figure 7b). In cross section, four lobes of the R8 cell body can be seen between the cell bodies of the regular retinula cells (Figure 7d). The cytoplasm of R8 is free of shielding pigment and most other cellular inclusions (Figures 7d). The rhabdom is surrounded by cisternae of smooth endoplasmic reticulum which form a pallisade around the rhabdom (Figure 7d). The pallisade forms a low refractive index layer around the rhabdom, resulting in the rhabdom acting as a light-guide (Horridge & Bernard, 1965). Groups of eight retinula cell axons penetrate the basement membrane below the rhabdoms.

Optics

Since the publication of Exner's (1891) work on optical mechanisms in insects and crustaceans, compound eyes have been routinely divided into apposition and superposition eyes. The existence of superposition optics was brought into question when Kuiper (1962) found that crayfish cones were of a low, more or less constant refractive index. This rendered them incapable of functioning as lens cylinders and thus apparently incapable of contributing to superposition image formation. Several authors subsequently questioned whether the superposition mechanism existed (reviewed by Horridge, 1975). The discovery of reflecting superposition optics (Vogt, 1975; Land, 1976) resolved the theoretical problems of image formation by cones of low refractive index. Image formation in superposition eyes has now been demonstrated in several species.

A superposition image is clearly formed by the eyes of *Nephrops norvegicus* as can be demonstrated using a modification of the technique of Land et al (1979). A reducing telescope is used to direct a fine beam of light onto the cornea, and the path of this beam inside the eye observed through a small hole cut in the cornea. The redirection of a series of parallel rays within the cone cell layer of a dark-adapted *N. norvegicus* eye is shown in Figure 8. When these rays are superimposed onto a diagram of the eye the focus can be seen to occur in the rhabdom layer (Figure 9). Spherical aberration is seen in those rays furthest from the optical axis, resulting in these rays being focused somewhat distally.

Eyeshine is a characteristic seen in most superposition eyes, that occurs when light is reflected back out of the eye by a tapetum without being absorbed during its passage through the rhabdoms (Figure 3a). The tapetum acts as a diffuse reflector, made up of reflecting pigment granules, and it enhances sensitivity by effectively doubling the length of the rhabdom. Eyeshine observations are of optical importance as the diameter of the eyeshine patch at the cornea represents the effective aperture of the superposition eye (Kunze, 1979).

In many crustacean superposition eyes, the distal pigment acts as an iris (Stavenga, 1979), reducing the diameter of the eyeshine patch during light adaptation through pigment migration. In *N. norvegicus*, with its non-migrating distal pigment, the width of the eyeshine patch remains relatively

constant, although the intensity decreases due to proximal pigment obscuring the tapetum (Figure 10).

Regional variations in the eyeshine of *N. norvegicus* are seen, due to two factors already mentioned: the kidney shape of the eye and the presence of shorter apposition ommatidia dorsally. When isolated dark-adapted eyes are photographed from various directions, variations are seen in both vertical and horizontal planes (Figure 11). The area of the eye decreased anteriorly and posteriorly from a maximum when the eye was viewed laterally (Figure 12a). When observed along dorsal to ventral axis, the apparent area of the eye fell symmetrically either side of the lateral view (Figure 12b). The manner in which the area of eyeshine varied with viewing angle differed in many ways from that in which the eye area varied. The most noticeable difference in the horizontal plane is that the area of eyeshine remains more or less constant over the region from 90° anterior to 60° posterior. At the anterior and posterior margins eyeshine area falls rapidly. In the vertical plane, the eyeshine area is as large only in the ventro-lateral part of the eye. Dorsally, the eyeshine decreases rapidly and is more or less absent 30° from the horizontal (Figure 12b).

A dorso-ventral gradient of eyeshine brightness is seen *N. norvegicus*, with the effective aperture of the eye varying from around 3,000 facets in the ventral half of the eye down to a single facet dorsally where apposition optics are apparently in use. For a strictly benthic animal such as *N. norvegicus*, most visually-mediated behaviour, such as territorial disputes, mate location and feeding, will occur at or below the horizontal. The distribution of bright eyeshine thus coincides with the regions of both greatest interest and least light. The dorsal region of reduced eyeshine occurs in that part of the eye viewing objects in silhouette against the relatively bright downwelling light.

Determining the path of light within the eye requires knowledge of the refractive indices (RI) of the active optical components of the eye. Interference microscopy has been used for many years in the determination of the RI of biological specimens (Hale, 1958). Several optical investigations have used the method to provide information on imaging systems in compound eyes. Apposition eyes have been studied in some depth, both in insects (eg. honey bee - Varela & Wiitanen, 1970) and in crustaceans

(*Artemia salina* - Nilsson & Odselius, 1981; *Cirolana borealis* - Nilsson & Nilsson, 1981), as have refracting superposition eyes (*Ephestia* - Cleary *et al*, 1977; euphausiids - Land & Burton, 1979; *Gennadus, Dardanus* and *Anaspides* - Nilsson, 1990) and reflecting superposition eyes (*Munida rugosa* - Gaten, 1994; crayfish - Vogt ,1977, 1980; *Cherax destructor* -Bryceson, 1981; *Macrobrachium rosenbergii* (Nilsson, 1983) using interference microscopy. However, the method has its limitations, especially in determining absolute, rather than differences in, RI (Kirschfeld & Snyder, 1975). The fact that due to their fragility it is necessary to use fixed, rather than fresh, material means that the precise RIs of most decapod eye components remain unknown.

Rhabdoms and fragments of cornea were isolated from lightly fixed eyes and the RI measured using the technique described in Gaten (1994)(Table 1). Cone stalks and attached crystalline cones were similarly isolated and the RI measured at intervals down the middle of the crystalline cones and the cone stalks. The RI of the crystalline cone is homogeneous over most of its length, decreasing sharply at the distal and proximal ends.

In the cone stalk, the RI decreases along a distal to proximal gradient (Figure 13). This RI gradient has been observed in other reflecting superposition eyes and approximately follows the function:

$$n_y = n_m \left[1 + \left(\frac{\sin \partial}{y + \cos \partial - 1} \right)^2 \right]^{1/2}$$

Where y is the relative distance from the distal end of the cone, ny is the refractive index at y, nm is the refractive index of the surrounding medium and ∂ is the angle between the sides of the cone (Vogt, 1977).

Table 1. Refractive index (mean and s.d. of n measurements) of cornea (measured in the centre and at the edge of the facets), crystalline cone and rhabdoms.

Location	RI	s.d.	n

Cornea -centre	1.425	0.004	35
Cornea - edge	1.420	0.003	35
Crystalline cone	1.412	0.007	12
Rhabdoms	1.365	0.010	25

The measured RI gradients of the crystalline cone cells approximately follow the theoretical curve (Figure 13). The latter assume that the external RI (nm) is 1.365 which is the value obtained for *N. norvegicus* cone cell cytoplasm (mean of 14 measurements, s.d. = 0.007). The only areas where the predicted curve differs markedly from the experimental curve are in the cone and at the proximal end of the stalk.

The RI values obtained from the middle region of the cones all fell within the range 1.41 to 1.44. This is in line with previously published results from reflecting superposition eyes such as those of the freshwater shrimp, *Macrobrachium rosenbergii* (Nilsson, 1983), and the crayfish *Astacus* (*Austropotamobius pallipes*) (Vogt, 1980).

A high RI in the distal stalk is necessary to ensure that rays of light passing through the cone without striking the sides are reflected by total internal reflection in the stalk. However, after a single reflection, either within the cone or the stalk, it is vital for the correct functioning of the eye that any rays leave the stalk when they next strike the wall lower down the stalk. To ensure that this happens, the RI gets progressively lower in more proximal regions of the stalk

Vogt's (1977) function relating the decrease in RI to distance down the cone and cone stalk agrees well with the experimental results, although in all cases the theoretical gradient is slightly higher than the measured values of RI. The value used for the RI of the surrounding medium (1.365) was probably too high as this was calculated using lightly fixed cells. The values used by Vogt (1977) were estimates of the RI of unfixed cytoplasm (1.34 and 1.35) and these resulted in the theoretical curve being rather lower than his experimental results. In the region of the cone/stalk junction, the RI required by the theoretical curves becomes unphysiologically high. Distal to this the cone can only contribute to the

superposition image by using an additional reflection mechanism. This role is fulfilled by the reflecting multilayer (Land, 1972) that lines the sides of the cones (Vogt, 1977).

The proximal end of the stalk had a higher RI than the mid-section. This has also been recorded in *Macrobrachium rosenbergii* (Nilsson, 1983). According to Nilsson (1983) this proximal increase in the RI serves to deflect stray light from the target rhabdom. This has the effect that light entering from another ommatidium is refracted at the tip of the stalk and forced to leave the opposite side of the rhabdom leading to a narrowing of the acceptance angle (Nilsson, 1983).

Spatial resolution in compound eyes is ultimately dependent on the interommatidial angle ($\Delta\varphi$), defined as the angular separation of the receptors. The method used was to photograph half-eyes, fixed and then cut along the midline. From these, the orientation of the cone axes can be determined accurately, in addition to the local radius of curvature of the eye. The best estimate of $\Delta\varphi$ obtained from photographs of fixed, bisected eyes was 0.94° (s.d. 0.1).

Although all eyes with high spatial resolution have small interommatidial angles, the presence of the latter in reflecting superposition eyes does not necessarily mean that spatial resolution is high. Even though *N. norvegicus* has a very low value of $\Delta\varphi$ (0.94°) direct observation of the superposition light path suggests that each rhabdom should receive light over a wide angle. The spatial resolution is thus dependent on factors other than $\Delta\varphi$ and is best determined by electrophysiology. Angular sensitivity functions were determined by intracellular electrophysiology (Shelton & Gaten, 1996). The acceptance angles (half width of the angular sensitivity function) were 11.3° in the dark adapted eye and 8.85° in the light adapted eye.

The discrepancy between the interommatidial angle ($\Delta\varphi$) and the acceptance angle ($\Delta\rho$) in *N. norvegicus* must lead to oversampling of the environment with several ommatidia viewing a single point in space. However, the ability of the eye to resolve detail depends not only on the anatomical distribution of the receptors, but also on the quality of the optics delivering the light to the receptors (Land, 1989). The spatial resolution determined electrophysiologically for the eyes of *N. norvegicus* suggests that resolving power is limited in these eyes by optical defects rather than anatomical

constraints such as receptor density and orientation. Such optical defects include spherical aberration (Land, 1981), imperfect superposition of light rays (Nilsson, 1989) and cross-over of rays within the rhabdom layer (Warrant & McIntyre, 1991).

Spherically symmetrical superposition eyes have the cone axes centred on the centre of curvature of the eye (Land *et al*, 1979). In *N. norvegicus* the radius of curvature of the cornea varies across the eye due to the lateral flattening of the eye. The paths of ray bundles across the eye, based on the optical data referred to above, can be visualised on a tracing of a longitudinal section of the eye (Figure 9). Every fifth cone axis (obtained from photographs of half-eyes) is drawn and the rays are plotted assuming that the angle of rays crossing the clear zone is equal to the angle between the incident ray and the ommatidial axis plus the cone taper angle. For both anterior and posterior regions of the eye a reasonably sharp focus is obtained in the distal part of the rhabdom layer (Figure 9a). Had all of the cone axes been centred on the same point (labelled C1 in figure), those rays closest to the centre of the eye would have been reflected to a point deeper in the rhabdom layer. However, these cones are centred somewhat deeper, leading to smaller anterior and posterior blur circles. The blur circles in these regions are estimated to have diameters of about 7 to 10 rhabdoms (~7 to 10°).

When the superposition of rays in the lateral part of the eye is plotted (Figure 9b) the predicted image is much worse. The crystalline cone layer is now centred much deeper within the eye (towards point C in figure), resulting in incoming light being focussed well below the surface of the rhabdom layer. As a result, the blur circle has a diameter of around 20 rhabdoms, covering an angle of 20°. This large blur circle is formed because the eye retains approximately the same interommatidial angle and radius of curvature of the rhabdom layer whilst decreasing the width of the clear zone. However, although there is a considerable reduction in spatial resolution as a result of the lateral flattening of the eye, its sensitivity in this region should not be affected as the amount of light entering the eye and the number of rhabdoms receiving the light remains unchanged.

In *N. norvegicus* the disadvantage of loss of resolution resulting from the lateral flattening of the eye is presumably of little importance in an animal active at low light levels.

The spatial resolving power of a compound eye depends on interommatidial angle, but is further related to three main factors: the photic range over which the animal is normally active, its mean velocity, and the tasks for which the eyes are normally used (Snyder et al 1977). *N. norvegicus* is active at low light levels, generally moves slowly, and does not use its eyes for fine discrimination so we would expect its eyes to be adapted for high sensitivity even though its ommatidial array suggests that potentially it is capable of high spatial resolution (Warrant, 2006).

A high interommatidial angle/acceptance angle ratio (such as described here for *N. norvegicus*) and neural pooling are typically seen in animals active at low light levels and both have been implicated in the evolution of neural superposition eyes (Nilsson and Ro, 1994). For any given interommatidial angle, a large acceptance angle will result in more photons being collected with a concomitant improvement in the signal to noise ratio; a smaller acceptance angle would reduce the visual overlap between adjacent ommatidia, improving the spatial resolution (Nilsson and Ro, 1994). It is apparent from this that the eye of *N. norvegicus* is adapted for high sensitivity.

Reflecting superposition eyes are usually spherically symmetrical in the horizontal plane, with the rhabdom layer, crystalline cone layer and the cornea sharing a common centre of curvature (e.g. *Munida* Gaten 1994). However, in *N. norvegicus* the eye is flattened laterally, resulting in the centre of curvature of the cornea and cones (but not the rhabdom layer) being displaced proximally and the lengths of the ommatidia in the middle of the eye being shortened; both of these combine to produce underfocussing, with the distance between the retina and the crystalline cones less than the focal length of the dioptric apparatus. This results in an obvious loss of resolution in spite of the small interommatidial angle. Underfocussing is seen in insect ocelli (Wilson, 1978; Schuppe & Hengstenberg, 1993; Berry et al., 2006) and in box jellyfish eyes (Nilsson et al, 2005) where poor quality images are produced in situations where advanced spatial information processing is not required.

Electrophysiology

Eyes function as matched filters in that they are adapted to extract the available, or important, spatial and spectral information out of the environment and to react as appropriate to temporally, and sometimes spectrally, varying signals. Evolution viewed through the lens of symmorphosis suggests that an understanding of the limitations of the eye in the spectral and temporal domains should provide some clues as to what they animal is looking for (Weibel et al, 1998). Compound eyes are generally accepted as being physiologically expensive (Laughlin, 1998). The large size of the eyes in absolute and relative terms therefore indicates their importance to *Nephrops*. As a major component of the sensory machinery it could be expected that they would be precisely adapted to meet the needs of the animal.

Ambient light availability in the marine environment is significantly impacted by a variety of factors other than the position of the sun and cloud cover. The initial interaction of light with water involves a transition between media of different refractive indices. Light striking a flat water surface is refracted so that it becomes more vertical, if there are at the air:water interface then the interaction becomes more complex and a temporal element becomes important as the waves move across the surface. The absorption of light as it passes through the water varies depending on the solutes and colloids suspended in it (Kirk, 1996). Generally coastal waters have plenty of detritus and gelbstoff in them so that light is absorbed fairly quickly with depth. The pigments in the water also drive the spectrum of light that does penetrate to any depth towards longer wavelengths. Reviewing the literature relating to spectral sensitivities of decapods, Johnson et al (2002) found that the pattern of spectral sensitivity matches that found in fish (Cronin, 1986, Partridge et al, 1992) with coastal species being more sensitive to longer wavelength light than deepsea or pelagic.

Electrophysiological recordings from *Nephorps norvegicus* appear to confirm evidence from histological examinations that the rhabdom consists of two sections with different spectral sensitivities (Figure 14). From other electrophysiological investigations, 16 species have been found to have both long and shortwave pigments (Johnson et al, 2002) and there are numerous other studies that indicate that most long bodied decapods probably have two photopigments (Eguchi et al, 1973; Cummins & Goldsmith, 1981; Gaten 1992; Frank & Widder, 1994a, 1994b, 1996; Johnson 1998). The

spectral sensitivities of *Nepgrops norvegicus* correspond very well with the spectra for coastal decapods generally. The presence of a shortwave pigment is particularly evident in light adapted *Nephrops norvegicus*, where the description of spectral sensitivity with one template (Stavenga et al, 1993) is particularly inadequate. In light adapted animals, where the relective tapetum is obscured by proximal pigments that coat the rhabdom except for the very distal tip (Figure 14 a,c), light passes through the rhabdom only once and the distal R8 rhabdomere thus contributes more to overall sensitivity. In dark adapted animals light passes twice through the proximal, longer wavelength sensitive region before reaching the distal shortwave region again. This is emphasised by the fact that in light adapted *Nephrops* the distal region appears to contribute 21% of the overall sensitivity curve while in dark adapted animals it is a mere 5% (Figure 14 b,d). The importance of the proximal region of the rhabdom layer in dark adapted animals may be enhanced by the afocal nature of the flattened lateral area of the eye as discussed above which may mean that light is focussed more proximally (Shelton et al, 1986).

Johnson (1998) suggests that the possession of two pigments allows decapods to be both sensitive to the most common wavelengths in their habitats (as per the sensitivity hypothesis of Munz, 1958) and to be able to pick out less dominant but arguably more important frequencies with their short wavelength pigments (Lythgoe, 1968). Gaten (1992) noted that in some decapods species the relative length of the distal shortwave receptor increased from dorsal to ventral. Looking upwards, marine organisms would be best to have enhanced sensitivity to silhouettes while laterally and ventrally shortwave bioluminescence would dominate the visual scene. The benthic infaunal crepuscular habit of *Nephrops* and the fact that it has a very broad depth range (10-800 m) may make the possession of two pigments useful in a range of situations. Short wavelength sensitivity may be useful in deeper water where there has been found to be an increase in bioluminescent activity near the sea bed (Craig et al, 2011), or generally as a mechanism for picking up on increased bacterial activity on detritus (Barak & Ulitzer, 1980).

The flexibility of ability in the eyes of *Nephrops* may also be an important factor with regard to their responses to temporally varying stimuli. Slow moving, deep sea animals, that inhabit a permanently

dark environment where downwelling light is of little importance have little need to adapt to varying background light intensities. Whatever they see is likely to be dim and important so having their eyes set to maximum sensitivity all the time is the best strategy. In shallower water there will be more natural variation in ambient light intensity over the day and much of what is visible is likely be unimportant. Animals in this situation need to have eyes that can be optimised for a range of conditions. For longer term variations in ambient light intensity the slow gain control provided by pigment movements will serve to ensure that the amount of light reaching the retinula cells maximises the information available and may protect the eye from damage though over-exposure (Gaten, 1990). Rapidly responding eyes are likely to be pointless in scotopic conditions where any dim object moving quickly is likely to be invisible no matter how effective the eyes are. It could actually be disadvantageous for an eye to adapt at all in low light conditions if gradual and small changes in light levels or slowly moving objects are important aspects of the visual scene. However in mesopic or photopic conditions where more light is available, shorter term background variations produced, e.g. by surface waves focussing light at depth (Čepič, 2008), more rapid gain control will be necessary to distinguish between ambient changes and superimposed changes in light intensity caused by objects moving across or appearing in the visual field. The compromise between the need to ignore low frequency changes in intensity and systemic limits on the ability to respond to high frequency modulations leads to band pass characteristics (McFarland & Loew, 1983). In a comparative studies of insects and decapods it has been found that there is generally a good match between the frequency which an eye responds to optimally and the ambient levels they are adapted for (Pinter, 1972; Howard, 1981; O'Carrol et al 1996; Moeller & Case, 1995). Animals from scotopic habitats tend to have 'low-pass' eyes that respond to small signals very strongly but slowly while animals from photopic habitats require greater changes in light intensity to demonstrate a response but respond more quickly. *Nephrops norvegicus* is able to shift between scotopic and mesopic modes, exhibiting sluggish sensitivity to all frequencies when dark adapted but optimal responses to 1-5 Hz when light adapted (Figure 16).

It is thought that this variation in response characteristic is mediated by various populations of pottasium ion channels in the rhabdom membranes that are responsible for repolarisation (Weckström & Laughlin, 1995). In dark adapted animals these channels open briefly in response to even very small depolarisations of the rhabdom. This leads to a slow repolarisation of the rhabdom. In the light adapted state a different population of potassium channels respond to depolarisations of 20-40 mV by remaining open until the rhabdom repolarises. It seems possible that part of the explanation for the insignificant input of the distal blue sensitive rhabdomere to the dark-adapted spectral sensitivity curve of *Nephrops* may be due to it being dominated by a light-adapted type population of potassium receptors.

Light-induced damage

The overwhelming majority of animals possess eyes and the loss of visual input in these animals is potentially disastrous. Acute light-induced damage can result through photothermal, photomechanical and photochemical mechanisms (Youssef et al 2011) and, although this can affect any animals exposed to excessive amounts of light, it is particularly dangerous for species whose eyes are adapted for high sensitivity. Deep sea crustaceans generally have eyes adapted for maximum sensitivity to light through the possession of eyes with large apertures and broad rhabdoms, and in the case of decapods through the use of superposition optics. Many such animals have been shown to exhibit photodamage when exposed to light levels beyond their ambient range, including the isopod *Cirolana borealis* (Nilsson & Lindstrom, 1983), krill *Meganyctiphanes norvegica* (Gaten et al, 2010) and vent shrimps *Rimicaris exoculata* (Herring et al, 1999). Photodamage in *Nephrops norvegicus* was first described by Loew (1976).

Nephrops norvegicus is particularly vulnerable to light-induced damage as, in addition to having very photosensitive eyes, it is the object of a significant fishery throughout Northern Europe (Johnson et al, this volume?). Following capture, undersized *N. norvegicus* are returned to the sea often after having been exposed to daylight. Short exposure to ambient daylight (as little as 9 min at 2.29×10^{20} photons $m^{-2}s^{-1}$) is sufficient to cause significant damage to the retinula cell layer (Shelton et al, 1985). In dark-adapted eyes more than 75% of the retinal cell layer is damaged by 15 s exposure to daylight.

Histological evidence of damage was visible as breakdown of the cell membranes and disruption of the rhabdom microvilli within 15 min of exposure; after 6 h, the retinula cell body layer is absent (Shelton et al, 1985). Animals fixed after being exposed to daylight for 2 h show complete loss of rhabdom structure and incursion of the shielding pigment (Figure 17B); one month later, the area is dominated by haemocytes with small amounts of disorganised membrane (Figure 17C).

Exposure of restrained animals to an artificial light source of known intensity reveals the time course of the retinal damage (Shelton et al., 1985). At high intensity ($6x10^{20}$ photons $m^{-2}s^{-1}$), 1 min exposure was sufficient to cause total retinal damage in dark-adapted eyes, whereas in light-adapted eyes only around 60% of the eye was damaged (Figure 18). In these experiments, exposure to a lower intensity ($1.5x10^{20}$ photons $m^{-2}s^{-1}$) left a small proportion of undamaged retina in both light and dark-adapted states (Figure 18a). The threshold at which damage is first detected was investigated by exposing restrained animals to lower light levels (Shelton et al., 1985). In dark-adapted animals, damage was detected at the lowest intensity used ($6x10^{18}$ photons $m^{-2}s^{-1}$), whereas in light-adapted animals the threshold was ($3x10^{19}$ photons $m^{-2}s^{-1}$) (Figure 18b). The proportion of the retina damaged by these 10 s exposures was directly proportional to the light intensity used (Shelton et al.,1985).

Although all *N. norvegicus* are susceptible to damage at relatively low light levels, the extent of the damage is dependent on the depth from which they were taken (Gaten et al, 1990), with animals caught at 18 m suffering 40% retinal damage compared to 80% in those from 135 m following the same light exposure (Figure 19). Animals from 18 m had around half of the concentration of proximal shielding pigment compared to those from 135 m, and these shielding pigments only migrated half as far up the rhabdoms during light adaptation in shallow-water animals compared to those from deeper water (Gaten et al, 1990). The shielding pigments protect the rhabdoms (Shelton et al, 1986) by screening the rhabdoms from excess light, by raising the refractive index adjacent to the rhabdom (thus reducing light retention by total internal reflection), and by isolating the tapetum (reducing the reflection of light back through the rhabdoms). As a result, the reduction in pigment concentration and the exposure of the distal half of the rhabdom both contribute to the increase in damage seen in

deep water animals. These differences between animals from different depths are unlikely to be due to genetic isolation as there is extensive mixing during the planktonic larval stages (Farmer, 1975).

However, even when these differences in screening pigment concentration and position are taken into account by exposing dark-adapted animals to light (with all of these pigments retracted below the reflective tapetum), there is still an increase in susceptibility to damage with depth (Gaten et al, 1990). Dark-adapted animals from all depths showed a positive correlation between light exposure and retinula cell damage. The visual pigment rhodopsin has been shown in mammals to be responsible for acute photodamage to the retina, probably due to the photosensitizing role of the all-trans-retinal chromophore found in rhodopsin (Rózanowska & Sarna, 2005). Sensitivity has been shown to depend on the rhodopsin content of a fly rhabdom (Razmjoo & Hamdorf, 1976), so a higher concentration of rhodopsin in the eyes of deep-water *N. norvegicus* would result in both increased sensitivity and greater susceptibility to light-induced damage. It has also been suggested (Loew, 1975) that the slow rate of visual pigment regeneration in this species might result in a loss of structural integrity in the photoreceptor membrane.

Maintaining *N. norvegicus* in constant darkness for 26 h before exposing them to damaging levels of light resulted in a significant decrease in the amount of damage, even though the shielding pigments remained in the dark-adapted state (Gaten et al, 1990). This may have been as a result of the interruption to the normal membrane turnover that is commonly seen in invertebrate rhabdoms (Fleissner & Fleissner, 2006). Alternatively, the protection of the rhabdoms may have occurred as a result of the release of heat shock proteins. These are produced in response to thermal stress or other metabolic shock in many taxa including crustaceans (Clark & Peck, 2009). They appear to provide protection for retinal cells against light-induced damage (Barbe et al, 1988).

Although photodamage is initially detectable only at the electron microscope level, within 15 min serious disruption of the rhabdoms and surrounding cells can be seen and after 6 h the retinula cell layer is completely disorganised (Shelton et al, 1985). This is followed by damage to the crystalline tracts that cross the eye (Figure 20a) with the result that they no longer fill the proximal clear zone (Gaten, 1988). The crystalline cones become variable in appearance and no longer display the precise

alignment seen in undamaged eyes. Around 2 months after exposure, the damage to the dioptric apparatus can be visualized externally in live *N. norvegicus*, appearing as a pale area when under infra-red illumination (Gaten, 1988). The damage is still apparent externally in animals recaptured one year (Figure 20 b,c) after exposure to light and sectioning of the eyes confirms that there is no recovery from retinal damage with time.

The effects of blinding on the ecology of *N. norvegicus* has been investigated by observation of individuals that were caught and tagged during daylight (Chapman et al, 2000) and by tagging and releasing animals following controlled exposure to artificial light (Shelton et al, 1985). Examination of tagged animals exposed to daylight (for around 5 min) and then recaptured up to 7 years later revealed a large range of eye damage, with 0% to 63.4% of the retina being destroyed (Chapman et al, 2000). No light measurements were taken at the times of capture or release so the variation in damage presumably relates to the ambient light at those times, the depth from which the animals were taken, and the degree of exposure to direct sunlight. Animals released and recaptured following controlled exposure to known levels of natural light (Shelton et al, 1985) showed a similar variation in retinal damage.

When exposed to intense artificial illumination, retinal damage was complete in the case of dark-adapted eyes and ranged from 5% to 100% in light-adapted eyes (median 56.4%) illustrating the protective value of the retinal shielding pigments (Chapman et al, 2000). *N. norvegicus* (both with intact vision and 100% retinal damage) were recaptured after 1 – 3 years and analysed for survival rate, growth rate and reproductive potential. Over the 8 years of the experiment, it was found that the survival of the animals was independent of the extent of eye damage and that there was no evidence that eye damage reduced growth rates. Although females showed a slightly higher survival rate than males, there was no significant change in the number of females carrying eggs (Chapman et al, 2000). It would appear that, in spite of investing in such a large eye, blind *N. norvegicus* survive, grow and reproduce as well as fully sighted individuals. However, the results may have been skewed due to the possibility that blinded individuals may have foraged for longer periods, leading to an increased likelihood of being recaptured.

The results of these studies clearly show that *N. norvegicus* are very susceptible to light-induced damage, particularly in the dark-adapted state, and that the damage is permanent. However, there is no evidence to suggest that this would have any effect on the fishery. It is important, though, to bear in mind the potential for eye damage when collecting or maintaining specimens for experimentation or for population studies.

Modelling the performance of the eye of *Nephrops*

Simple models that estimate the performance of the eye as a single unit have been developed and modified over the years. The accepted equation that describes the ratio of the number of photons absorbed per receptor to the number emitted per steradian from an extended source that are absorbed is:

$$S = (\pi / 4)^2 D^2 (d / f)^2 \left[\frac{kl}{2.3 + kl} \right]$$

Where D = the diameter of the aperture, l = length of the photoreceptor, k = the absorption coefficient of the rhabdom, d is the rhabdom diameter and f the focal length (Kirschfeld, 1974; Land, 1981; Warrant & Nilsson, 1998). However, while these models are adequate as a description of sensitivity, they may not capture the complexities of sensitivity under a range of internal pigment distributions and say nothing about resolution (or its relationship to sensitivity). Warrant & McIntyre (1991) pointed out that even if a superposition eye was perfectly focussed, because of the large aperture and correspondingly low F number, light from the periphery of the aperture would enter the target rhabdom at such an angle that light would bleed into adjacent rhabdoms thus degrading spatial resolution. Various solutions have evolved to deal with this problem including partial and complete sheaths of tapetal or shielding pigment and rhabdom morphology (Figure 21). *Nephrops norvegicus* has rhabdoms with pointed distal tips that have been estimated to supplement the angle that light can be accepted over by about 12.5 degrees.

Using basic trigonometry it is possible to estimate the extent of the blur circle based on the refraction of light by the diotric layer and the relationship between the radius of curvature of the rhabdom layer and the focal length (Figure 22). If we assume a spherical eye, its diameter and the aperture diameter can be used to estimate the angle of incidence of light at the periphery of the aperture (theta). To calculate the point where light from the periphery of the aperture is incident on the distal region of the rhabdom layer (R) the angle at which light is redirected by the dioptric layer (beta) must be known. This can be calculated by applying Snell's law and assuming the refractive indices of sea water (1.35; Kirk, 1983) and crystalline cones (1.42; Gaten, 1992) and accounting for the taper due to the interommatidial angle ($\Delta\varphi$):

$$\beta = \text{Sine}^{-1}(0.95 \text{ Sin } \theta) + \Delta\varphi$$

Since we know r, p and β we can apply the Sine rule for triangles:

$$\delta = 180 - \text{Sine}^{-1}(r \sin \beta \, p^{-1})$$

And the angle (σ) that defines the edge of the blur circle can be calculated as

$$\sigma = \delta + \alpha - 180$$

Based on these assumptions and from measurements of *Nephrops* eyes discussed above it is possible to estimate the extent of the blur circle at the anterior and lateral regions of the eye. The calculations based on anatomical measurements show good agreement with the diagrammatic ray-tracing approach, suggesting a larger blur circle laterally.

Table 2 parameters for anterior and lateral regions of the eye of *Nephrops norvegicus*

Parameter	**Lateral**	**Anterior**
Inerommatidial angle ($\Delta\varphi$)	0.73°	0.84°
Radius of curvature of the eye (r)	3.9 mm	3.4 mm
Radius of curvature of retina (p)	2.8 mm	2.0 mm
Aperture radius	1.60 mm	1.53 mm

Blur circle extent (σ)	12.6°	8°
Blur circle extent (ommatidia)	17	10

To explore the implications of the variation in eye parameters on sensitivity and resolution of superposition compound eyes a ray tracing model has been developed using the programming language Python (Johnson, 1998, Johnson & Moss, in prep). This model initially assumes that super-imposed light coming from a single facet will land on a single rhabdom and uses a combination of anatomical measurements and estimated parameters (Table 2) to calculate the distribution of light to and within the rhabdom layer. The model takes account of the blur circle extent, absorbance of light by the photopigments and the interaction of light with shielding and reflecting pigments. It also accounts for the decreased per facet contribution of light towards the periphery of the aperture and behaviour of light within rhabdoms depending on reflecting/tapetal pigment extent and whether it is assumed that they are flat or tapered distally.

Both the lateral and anterior regions of the eye were modelled using the parameters in Table 2. Rhabdom dimensions of 180µm length and 25 µm width and a facet diameter of 50 µm were assumed to be constant (Johnson, 1998). The model suggests that the presence of any sort of tapetum in *Nephrops* improves sensitivity by about 10% but that increasing extent of reflective pigment along the rhabdom may actually reduce sensitivity (Figure 22a-c). This is likely to be a result of light passing between adjacent rhabdoms when the tapetum is basal so that light has a longer pathlength through photopigment. However, increasing tapetal extent does improve resolution. There is a clear impact of shielding pigment on sensitivity in both lateral (Figure 22d,e) and anterior regions of the eye (Figure 22f). Despite the fact that the aperture of the lateral region is only slightly larger than anteriorally, the model suggests that the combination of a larger blur circle, smaller interommatidial angle makes about 10% more sensitive. It is notable, comparing figures for lateral and anterior regions of the eye that the relative contribution of the axial rhabdom to overall sensitivity is much less laterally compared with the anterior region of the eye.

It is likely that this difference can be linked to the smaller blur circle and much better resolution in the anterior region of the eye. The predicted resolution in this region approaches 5.5° for a fully sheathed rhabdom compared with a best of around 10° laterally. This is due to the more appropriate relationship between the radii of cornea and rhabdom layers. The model suggests that while the possession of pointed rhabdoms results in a slight improvement in sensitivity in the poorly focussed lateral region of the eye, it may actually be detrimental to resolution. This is a consequence of the rhabdoms within the larger blur circle individually more effectively capturing incident light. This makes the profile of absorbance across the retina broader and flatter than is the case with flat ended rhabdoms. In the anterior region of the eye the possession of pointed rhabdoms appeared to have minimal effect. This is because very little light arrives at the distal tips of rhabdoms at an angle greater than 12.5°. In summary, the ray tracing model appears to confirm the suggestion that the anterior and lateral areas of the eye have very different capacities and are likely to serve slightly different functions. It seems that the lateral flattening of the cornea of *Nephrops* could serve some advantage rather than simply represent a relaxation of evolutionary pressure in the absence of specific function.

1. Eye structure and Optics: a description of the unusual structure of one of the largest crustacean eyes, and how the structure leads to the unique optical arrangement found in this species.
2. Optical Physiology: electrophysiological investigations into the resolution, temporal and spectral sensitivity of the eye have revealed the visual capabilities of this species. Eyeshine.
3. Light-induced damage: the well documented susceptibility to blinding during normal capture and handling procedures leads to problems both with commercial sustainability (following the return of undersized individuals) and with any scientific experimentation on the species.

References

Arechiga, H & Atkinson, R.J.A. (1975). The eye and some effects of light on locomotor activity in *Nephrops norvegicus*. Marine Biology, 32(1), 63-76

Barak, M & Ulitzer, S. (1980) Bacterial bioluminescence as an early indicator of marine fish spoilage. European Journal of Applied Microbiology, **10**, 155-165

Barbe MF, Tyrell M, Gower DJ & Welch WJ 1988. Hyperthermia protects against light damage in the rat retina. Science **241**, 1817-1820.

Berry, R.P., Warrant, E.J. and Stange, G. (2007). Form vision in the insect dorsal ocelli: an anatomical and optical analysis of the locust ocelli. Vision Res. 47, 1382-1393.

Bryceson, K.P. (1981). Focusing of light by corneal lenses in a reflecting superposition eye, Journal of experimental biology, 90,347-350

Čepič, M. (2008) Underwater rays. European Journal of Physics, **29**, 845-855

Chapman C.J., Shelton P.M.J., Shanks A.M. & Gaten E. (1989) Tagging experiments on *Nephrops* in a Scottish loch. International Council for the Exploration of the Sea, CM 1989/K:6. 9pp.

Chapman C. J., Shelton P.M.J., Shanks A. M. & Gaten E. (2000) Survival and growth of the Norway lobster, *Nephrops norvegicus* (L.), in relation to light-induced eye damage. Marine Biology **136**, 233-241.

Clark MS & Peck LS (2009). HSP70 heat shock proteins and environmental stress in Antarctic marine organisms: a mini-review. *Marine Genomics* **2**, 11-18.

Cleary, P., Deichsel, G. & Kunze, P (1977). The superposition image in the eye of *Ephestia kühniella*, journal of Comparative Physiology A, 119(1),73-84

Craig, J., Jaimeson, A.J., Bagley, P.M. & Priede, I.G. (2011). Naturally occurring bioluminescence on the deep-sea floor. Journal of Marine Systems. **88**(4), 563-567

Cronin, T. (1986) Optical design and evolutionary adaptation in crustacean compound eyes. Journal of Crustacean Biology, **6**(1), 1-23

Cummins, D. & Goldsmith, T.H. (1981). Cellular identification of the violet receptor in the crayfish eye. Journal of Comparative Physiology. **142**, 199-202

Eguchi, E., Waterman, T.H. & Akiyama, J (1973) Localization of the violet and yellow receptor cells in the crayfish retina. Journal of General Physiology, **62**, 355-374

Exner, S. (1891) The Physiology of the Compound Eyes of Insects and Crustaceans (R.C. Hardia, Translator). Berlin, Springer-Verlag

Farmer, A.S.D. (1975) Synopsis of data on the Norway lobster, *Nephrops norvegicus*. FAO Fisheries Synopsis No. 112, 1-97

Fleissner, G. and Fleissner, G. (2006). Endogenous control of visual adaptation in invertebrates. In "Invertebrate Vision" (E.J. Warrant and D.E. Nilsson, eds.) Cambridge: University Press.

Frank, T.M. & Widder, E.A. (1994) Comparative study of behavioural sensitivity thresholds to near UV and blue-green light in deep-sea crustaceans. Marine Biology, **121**, 229-235

Frank, T.M. & Widder, E.A. (1994) Evidence for behavioural sensitivity to near-UV light in the deep-sea crustacean *Systellaspis debilis*. Marine Biology, **118**, 279-284

Frank, T.M. & Widder, E.A. (1996) UV light in the deep-sea: *in situ* measurements of downwelling light in relation to the visual threshold sensitivity of UV-sensitive crustaceans. Marine and Freshwater Behaviour and Physiology, **27**, 189-197

Gaten E. & Shelton P.M.J. (1993) Spatial resolution in benthic decapods, determined by electrophysiological measurement of acceptance angle. Journal of Physiology, **467**, 371P.

Gaten E. (1988) Light-induced damage to the dioptric apparatus in *Nephrops norvegicus* and the quantitative assessment of the damage. Marine Behaviour and Physiology, **13**, 169-183.

Gaten E. (1992) The anatomy and physiology of selected reflecting superposition eyes. PhD thesis. University of Leicester, 203 p.

Gaten, E. (1990) The ultrastructure of the compound eye of *Munida rugosa* (Crustacea: Anomura) and pigment migration during light and dark adaptation. Journal of Morphology, **205**, 243-253

Gaten E. (1994) Geometrical optics of a galatheid compound eye. Journal of comparative Physiology A, **175**, 749-759.

Gaten E. (1998) Optics and phylogeny: is there an insight? The evolution of superposition eyes in the Decapoda (Crustacea). Contributions to Zoology **67**, 223-235.

Gaten E., Shelton P.M.J., Chapman C.J. & Shanks A.M. (1990) Depth-related variation in structure and functioning of the compound eyes of the Norway lobster *Nephrops norvegicus*. Journal of the Marine Biological Association, **70**, 343-355.

Gaten, E., Wiese, K. & Johnson, M.L. (2010) Laboratory based observations of behaviour in northern krill (*Meganyctiphanes norvegica* Sars*)*. Advances in Marine Biology, **57**, 233-255.

Hafner, G.S., Tokarski, T.R., 1998. Morphogenesis and pattern formation in the retina of the crayfish *Procambarus clarkii*. Cell and Tissue Research **293**, 535-550.

Hafner G.S. & Tokarski T.R. (2001) Retinal development in the lobster *Homarus americanus*: comparison with compound eyes of insects and other crustaceans. Cell Tissue Research, **305**, 147-158.

Hale, A.J. (1958). The Interference Microscope in Biological Research. E.S. Livingstone, 114 pp

Harzsch S & Hafner G.S. (2006) Evolution of eye development in arthropods: phylogenetic aspects. Arthropod Structure and Development, **35**, 319-340.

Herring P.J., Gaten E. & Shelton P.M.J. (1999) Are vent shrimps blinded by science? Nature, **398** 116.

Horridge, G.A. (1975) Optical mechanisms of clear-zone eyes. In: The Compound Eye and Vision of Insects (Ed. G.A. Horridge), pp 255-298, Oxford, Clarendon

Howard, J. (1981). Temporal resolving power of the photoreceptors of *Locusta migratoria*. Journal of Comparative Physiology, **144**, 61-66

Johnson, M. L. (1998). Aspects of vision in mesopelagic decapods. University of Leicester. PhD Thesis

Johnson M.L, Gaten E. & Shelton P.M.J. (2002) Spectral sensitivities of five marine decapods crustaceans and a review of spectral sensitivity variation in relation to habitat. Journal of the Marine Biological Association, **82**, 835-842.

Johnson M.L, Shelton P.M.J. & Gaten E. (2000) Temporal resolution in marine decapods from coastal and deep-sea habitats. Marine Biology **136**, 243-248.

Kirk, J.T.O. (1996) Light and Photosynthesis in Aquatic Ecosystems. Cambridge University Press, Cambridge

Kirshfeld, K. (1974). The absolute sensitivity of lens and compound eyes. Z. Natureforsch, 29c, 592-596

Kirschfeld, K. and Snyder, A.W. (1975). Waveguide mode effects, birefringence and dichroism in fly photoreceptors. *In* "Photoreceptor optics" (A.W. Snyder and R.Menzel, eds.) Berlin, New York: Springer-Verlag.

Kleinholz, L.H. (1961) Pigmentory effectors. In: The Physiology of Crustacea, Vol 2 (Ed. T.H. Waterman) pp133-169. New York, Academic Press.

Kuiper, J.W. (1962) The optics of the compound eye. Symposia of the Society for Experimental Biology, 16,58-71

Kunze, P. (1979) Apposition and superposition eyes. In: Handbook of Sensory Physiology, VII/6A (Ed. H. Autrum), pp 441-502, Berlin, Springer-Verlag

Land, M.F. (1972). The physics and biology of animal reflectors. Progress in Biophysics and Molecular Biology, 24,75-106

Land, M.F. (1976). Superposition images are formed by reflection in the eyes of some oceanic decapod Crustacea. *Nature*, 263:764-765

Land, M.F. (1981) Optics and vision in invertebrates. In: Handbook of Sensory Physiology, VII/6B (Ed. H. Autrum), pp471-492, Berlin, Springer Verlag

Land, M.F. (1989). Variations in the structure and design of compound eyes. In: Facets of Vision (Ed. D.G. Stavenga & R.C. Hardie) pp 90-111, Berlin, Springer-Verlag

Land, M.F. & Nilsson, D.-E. (2002). Animal Eyes. Oxford University Press, Oxford.

Land, M.F. & Burton, F.A. (1979). The refractive index gradient in the crystalline cones of the eyes of a euphausiid crustacean. Journal of Experimental Biology, 82:395-398

Land, M.F., Burton, F.A. & Meyer-Rochow, V.B. (1979). The optical geometry of euphausiid eyes. Journal of Comparative Physiology, 130,49-62

Laughlin,S.B., de Ruyter van Stevenwick, R.R. & Anderson, J.C. (1998) The metabolic cost of information. Nature Neuroscience, 1(1):36-41

Loew E R. 1976 Light, and photoreceptor degeneration in the Norway lobster *Nephrops norvegicus* (L.) Proceedings of the Royal Society London B, **193**, 31-44.

Lythgoe, J.N. (1968) Visual pigments and visual range under water. Vision Research, **8**, 977-1012

McFarland, W.N. & Loew, E.R. (1983) Wave induced changes in underwater light and their relation to vision. Environmental Biology of Fish, **8**, 173-184

Moeller, J.F. & Case, J.F. (1995) Temporal adaptations of visual systems in deep-sea crustaceans. Marine Biology, **124**, 47-54

Munz, F.W. (1958) Photosensitivie pigments from the retinae of certain deep-sea fishes. Journal of Physiology, **140**, 220-235

Nilsson, D.E. (1983). Evolutionary links between apposition and superposition optics in crustacean eyes. Nature 302,818-821

Nilsson, D.E. (1989) Optics and the evolution of the compound eye. In Facets of Vision (Ed D.G. Stavenga & R.C. Hardie), pp 30-73 Berlin, Springer-Verlag.

Nilsson, D.E. (1990). Three unexpected cases of refracting superposition eyes in crustaceans. Journal of Comparative Physiology A, 167, 71-78

Nilsson, D.-E., Gilsén, L., Coates,M., Skogh, C. and Garm, A. (2005). Advanced optics in a jellyfish eye. Nature 435, 201–205.

Nilsson, D.E. & Nilsson, H.L. (1981). A crustacean compound eye adapted for low light intensities (Isopoda). Journal of Comparative Physiology, 143, 503-510

Nilsson, D.E. & Odselius, R. (1981). A new mechanism for light-dark adaptation in the *Artemia* compound eye. Journal of Comparative Physiology, 143,389-399

Nilsson, H.L. & Lindstrom M. 1983 Retinal damage and sensitivity loss of a light-sensitive crustacaean compound eye (*Cirolana borealis*). *Journal of Experimental Biology,* **107**, 277-292.

Nilsson, D. E. and Ro, A.I. (1994). Did neural pooling for night vision lead to the evolution of neural superposition eyes? J. Comp. Physiol. A, 175, 289-302.

O'Carroll, D. C., Bidwell, N. J., Laughlin, S. B., & Warrant, E. J. (1996) Insect motion detectors matched to visual ecology. Nature, 382, 63–66.

Parker, G.H. (1932) The movements of retinal pigment. Ergbn. Der Biol. Bd. 9, pp 239-291

Parker, G.H. (1890). The histology and development of the eye of the lobster. Bull. Mus. Comp. Zool. Harvard University, 20,1-60

Partridge, J.C., Archer, S.N. & van Oostrum, J. (1992). Single and multiple visual pigments in deep sea fishes. Journal of the Marine Biological Association UK, **72**, 113-130

Pinter, R.B. (1972) Frequency and time domain properties of retinular cells of the desert locust (*Schistocerca gregaria*) and the house cricket (*Acheta domesticus*) Journal of Comparative Physiology, **77**, 383-397

Razmjoo S & Hamdorf K. 1976 Visual sensitivity and the variation of total photopigment content in the blowfly photoreceptor membrane. Journal of Comparative Physiology A, **105**, 279-286.

Rózanowska M & Sarna T, 2005 Light-induced damage to the retina: role of rhodopsin chromophore revisited. Photochemistry and Photobiology, **81** 1305-1350.

Schuppe, H. and Hengstenberg, R. (1993). Optical properties of the ocelli of *Calliphora erythrocephala* and their role in the dorsal light response. J. Comp. Physiol. A, 173, 143–149.

Shelton P.M.J. & Gaten E. (1996) Spatial resolution determined by electrophysiological measurement of acceptance angle in two species of benthic decapod crustacean. Journal of the Marine Biological Association, **76**: 391-401.

Shelton P.M.J., Gaten E. & Chapman C.J. (1985) Light and retinal damage in *Nephrops norvegicus* (L.). Proceedings of the Royal Society of London B., **226**, 217-236.

Shelton P.M.J., Gaten E. & Chapman C.J. (1986) Accessory pigment distribution and migration in the compound eye of *Nephrops norvegicus* (L.) (Crustacea: Decapoda). Journal of experimental marine Biology and Ecology, **98**, 185-198.

Shelton P.M.J., Gaten E. & Chapman C.J. (1989) Light-induced retinal damage in *Nephrops norvegicus* (L.). Journal of the Marine Biological Association, **69**, 737.

Shelton, P.M.J., Shelton, R.G.J. & Richards, P.R. (1981). Eye development in relation to moult stage in the European lobster, *Homarus gammarus* (L.) Journal du Conseil, 39:239-243

Snyder, A.W., Stavenga, D.G. and Laughlin, S.B. (1977). Spatial information capacity of compound eyes. J. Comp. Physiol. A, 116, 183-207.

Stavenga, D.G. (1979) Pseudopupils of compound eyes. In: Handbook of Sensory Physiology: Vision in Invertebrates, VII/6A (Ed H. Autrum), pp 357-502, Berlin, Springer-Verlag

Stavenga, D.G., Smits, R.P. & Hoenders, B.J. (1993)

Tokarski, T.R. & Hafner, G.S. (1984). Regional morphological variations within the crayfish eye. Cell and Tissue Research, 235:387-392

Valera, F.G. & Wiitanen, W. (1970). The optics of the compound eye of the honeybee (*Apis mellifera*). Journal of General Physiology, 55,336-358

Vogt, K. (1975). Optik des flubkrebsauges. Zeit. Natur. 30c, 691

Vogt, K. (1977). Ray path and reflection mechanisms in crayfish eyes. Z. Naturforsch, 32, 466-468

Vogt, K. (1980). Die Spiegeloptik des Flussjrebsauges, Joutnal of Comparative Physiology, 135,1-19

Warrant, E.J. (2006) Invertebrate vision in dim light. In "Invertebrate Vision" (E.J. Warrant and D.E. Nilsson, eds.). Cambridge: University Press.

Warrant, E.J. & McIntyre, P.D. (1991). Strategies for retinal design in arthropod eyes of low F-number. Journal of Comparative Physiology A, 168:499-512

Weckström, M. & Laughlin, S.B. (1995). Visual ecology and voltage gated ion channels in insect photoreceptors. Trends in Neurosciences, **18**, 17-21

Weibel, E.R.C., Taylor, C.R. & Bolis, L. (1998) Principles of Animal Design: The Optimization and Symmorphosis Debate. Cambridge, Cambridge University Press

Wilson, M. (1978). The functional organisation of locust ocelli. J. Comp. Physiol. A, 124, 297–316.

Youssef PN, Sheibani N & Albert DM 2011 Retinal light toxicity. *Eye (Lond)* **25**, 1-14.

Figure legends

Figure 1. A: Schematic diagram of a cross section through several ommatidia of an apposition compound eye as found in many arthropods. Light from a particular direction will only be detected by the photoreceptive rhabdom if is passes through the axial facet. B: A schematic demonstrating the principle of a reflecting superposition compound eye as found in *Nephrops norvegicus* and many other long bodied decapods. Parallel light is reflected by the multilayer reflectors along the edges of the crystalline cone cells towards the axial rhabdom, thuse several facets redirect light to the appropriate photoreceptor.

Figure 2. A: Lateral view of a dark-adapted eye showing oval shape, square facets and brilliant eyeshine. B: Longitudinal section through a fixed eye to show the increased length of ommatidia anteriorly (A) and posteriorly (P). The clear zone (cz) extends from the rhabdom layer (r) to the cone layer (marked by the dark distal shielding pigment). C: In this transverse section of the eye the gradual increase in ommatidial length from dorsal (D) to ventral (V) can be seen. D: Electron micrograph of the reflecting multilayer (rm) in a transverse section of the mid-cone region. The reflecting layers are separated by smooth endoplasmic reticulum (ser) and cytoplasm. c - crystalline cone, cce - corneagenous cell extension, dsp - shielding pigment granules. E: phase contrast micrograph showing shielding pigment in the distal pigment cells between the crystalline cones. F: polarizing micrograph of the same section showing the birefringent reflecting multilayer in the distal pigment cells. (Scale bars - A, B, C = 1.0 mm; D = 1.0 μm; E, F = 50 μm)

Figure 3. A: Light micrograph of a dark-adapted eye showing fusiform rhabdoms (r), backed by tapetal cells (t). The proximal shielding pigment (psp) is withdrawn behind the tapetal cells, close to the basement membrane. B: In this light micrograph two of the lobes of retinula cell 8 (R8) can be seen

either side of the distal rhabdom (dr) just below where the crystalline tract (ct) divides. The cytoplasm of R8 is noticeably free of cellular inclusions, compared to the surrounding retinula cells (R1-R7). C: Light microscopy of this transverse section at the distal rhabdom level shows the rhabdoms surrounded by four lobes of cell R8 and by the retinula cells (R1-R7). The cone cell processes (cp) lie at the corners of the distal rhabdoms. D: The banded appearance of the main rhabdom, seen in this electron micrograph of a longitudinal section, is due to orthogonally arranged layers of microvilli. E: The tapetal cells are packed with reflecting pigment granules (rp) which surround the rhabdom (r) closely in places. A cone process (cp) can be seen in this longitudinal section passing proximally between the tapetal cells. F: The retinula cell axons (a) pass through the basement membrane (bm). The cone cell processes (cp) rejoin and anchor to the basement membrane. In this longitudinal section of a dark-adapted ommatidium the proximal shielding pigment (psp) is close to the basement membrane. (Scale bars - A = 100 µm; B, C = 10 µm; D = 0.2 µm; E = 1.0 µm; F = 5 µm).

Figure 4: A) Semi-schematic diagram of a group of ommatidia from the eye of *Nephrops norvegicus*, shown in the light-adapted (LA) and dark-adapted (DA) states. The main difference between the two adaptional states is that the proximal shielding pigment migrates from around the basement membrane to a position higher up the rhabdom layer. B) An enlarged view of part of a distal pigment cell between two crystalline cones. Distal shielding pigment granules and a reflecting multilayer are present within the distal pigment cells. C) Semi schematic diagram of a first zoeal eye demonstrating that at this stage it resembles an apposition type eye.

Figure 5: Embryonic eye development in *N. norvegicus*. A) The gradient of ommatidial size from posterior (P) to anterior (A) can be seen in this light micrograph. B) At the posterior eye margin, epidermal cells become elongate (arrowed) and appear to extend from the cornea to the basement membrane (bm). Anterior to this is the region where differentiation of the cells and rhabdom formation occurs (bracketed). C) Electron micrograph of the region of differentiation. Distal invaginations (di) of the cornea occur where clusters of retinula cells sink away from the cornea. D) The square clusters of retinula cells are found in the most posterior part of the region marked with a bracket in B. E) The seven main retinula cells become wedge-shaped in transverse section, eventually interdigitating in the centre to form a presumptive rhabdom. The retinula cell R8 is positioned to one side of the main cluster. F) The most mature (anterior) ommatidia found in the embryos are similar in structure to those seen in the larval eye. The distal cone cell layer is largely filled with cone cells (c) and retinula cell nuclei (rcn). The rhabdom (r) layer is heavily pigmented from the level of the retinula cell nuclei down to the basement membrane (bm). (Scale bars - A = 200 µm; B = 100 µm; C, D, E = 2.0 µm; F = 100 µm).

Figure 6. Eye structure in the first zoea of *N. norvegicus*. A) Light micrograph of a longitudinal section through the eye showing the gradient of ommatidial size from posterior (P) to anterior (A). bm - basement membrane; c - cone cell; f - corneal facet; rcn - retinula cell nuclei; r - rhabdoms. B) Electron micrograph of the region where the cone cells abut the rhabdom. The difference in size can be seen between the proximal shielding pigment (psp) that surrounds the rhabdoms, and the large shielding pigment grains (lsp) that form the pigment shield above the rhabdom layer. C) Electron micrograph of a rhabdom in LS showing alternating layers of orthogonally-orientated microvilli as seen over most of the length of the rhabdom. D) Just proximal to the distal rhabdom, seven large retinula cells (1 - 7) and four lobes of R8 (8) are found around the rhabdom. Cone cell processes (arrowed) extend down to the basement membrane between the retinula cells. The rhabdom is surrounded by a

pallisade of expanded cisternae of smooth endoplasmic reticulum. (Scale bars - A = µm; B = 1.0 µm; C = µm; D = 1.0 µm).

Figure 7: A narrow beam of light is redirected at the crystalline cone layer to a superposition focus. The eye has been rephotographed at intervals as the beam is traversed across the eye. The light is redirected to the same region of the retinula cell layer. The beam is made visible by the addition of fluorescein to the seawater. (Scale bar = 2 mm).

Figure 8: A) Diagrammatic longitudinal section of the eye of N. norvegicus, showing parallel rays incident at 60° anterior (A) and posterior (P). The ommatidial axes ($\Delta\varphi$ = 1°; every 5th axis shown) converge towards the local centre of curvature of the eye which lies between C and C1. Cones closer to the centre of the eye are centred more deeply. They thus focus rays more distally than if they were centred at C1, thereby improving the quality of the focus (thicker dotted lines show ray paths if centred at C1). B) Diagrammatic longitudinal section of the eye of N. norvegicus, showing parallel rays incident on the central part of the eye. The ommatidial axes ($\Delta\varphi$ = 1°; every 5th axis shown) converge towards the local centre of curvature of the eye which lies between C and C1. The rays are focused much deeper within the rhabdom layer than is the case with anterior and posterior rays.

Figure 9. Variation in eyeshine patch diameter and intensity after exposure to daylight. Eyeshine intensity decreases rapidly but the diameter of the eyeshine patch remains fairly constant.

Figure 10: Photographs of eyeshine in an isolated, dark-adapted *N. norvegicus* eye, at 45° intervals from dorsal to ventral (D to V) and from anterior to posterior (A to P). Although there is a clear contrast between the dorsal and ventral eyeshine, around the horizontal axis the eyeshine is relatively uniform. Scale bar = 5 mm.Figure

Figure 11: Variation in apparent eye area and eyeshine area along a) the antero-posterior axis and b) the dorso-ventral axis.

Figure 12: Variation in refractive index along the cone stalk from the region abutting the crystalline cone (0) to the most proximal part that connects to the rhabdom(1).

Figure 13: Spectral sensitivities of *Nephrops norvegicus* (n=4) in the light-adapted (A, C) and dark-adapted (B, D) conditions. Figures 13 A and B depict the overall sensitivity curve based on contributions from two pigments. Figures 13 C and D show the separate absorption templates (Stavenga et al, 1993) that contribute to the combined curve. Redrawn from Johnson et al (2002)

Figure 14: Temporal sensitivities of *Nephrops norvegicus* (n=3) in the light-adapted and dark adapted conditions stimulated with a light varying in intensity sinusoidally. 14 A shows that eyes have reduced lag in the light adapted state. 14 B shows that dark-adapted eyes respond most to low frequency signals while light-adapted eyes demonstrate band-pass characteristics. Redrawn from Johnson et al (2000)

Figure 15: A) electron micrograph of an undamaged rhabdom showing alternating layers of microvilli cut in transverse and longitudinal section. Shielding pigment granules can be seen along the edge of the rhabdom. Scale bar = 1µm. B) After 2 h in daylight, the regular array of microvilli has broken down and shielding pigment is found within the rhabdom. Scale bar = 1µm. C) In eyes fixed 1 month after exposure, only a few membrane whorls remain where the rhabdom had been, together with haemocytes containing shielding pigment granules. Scale bar = 2µm.

Figure 16: A) Time course of damage to the retinula cell layer caused by exposure to tungsten light at 1000 (o) and 250 (filled circles) µmol $m^{-2}s^{-1}$ (1 µmol $m^{-2}s^{-1}$ = 6.023 x10^{17} photons $m^{-2}s^{-1}$) in both light-adapted (dotted lines) and dark-adapted (solid lines) states. Each point represents one or two eyes. B) Threshold for damage to the retinula cell layer; exposure of dark-adapted (filled circles) and light-adapted (o) eyes for 10 s to tungsten light of various intensities. Each point represents one eye. Figures redrawn from Shelton et al., 1985.

Figure 17: Retinal damage plotted against log photon fluence rate (1 µmol $m^{-2}s^{-1}$ = 6.023 x10^{17} photons $m^{-2}s^{-1}$) for animals taken from three different depths. At each depth, animals were exposed 2h (triangles), 4h (circles) and 26h (squares) after capture. Each point is the mean of 2 to 5 animals. Redrawn from Gaten et al., 1990.

Figure 18. A - an unfixed eye bisected two months after light damage, showing the absence of retinula cells centrally (**), retraction of the crystalline tracts and redistribution of the distal shielding pigment (DG). B - whole *N. norvegicus* eye from an animal recaptured one year after exposure to sunlight. The regular array of undamaged dorsal facets (**) can be contrasted with the darker, indistinct appearance of damaged areas. C - individual damaged ommatidia (arrowed) are identifiable by their darker appearance. All scale bars = 1 mm.

Figure 19: The fate of light-rays when they encounter a rhabdom. A) Passage through the target rhabdom to those adjacent, B) Reflection by the tapetum, C) Reflection by total internal reflection at the edge of the rhabdom due to differences in refractive index between the rhabdom and surrounding cytoplasm D) Absorption by proximal shielding pigment (enhanced by equal refractive indices), E) Total internal reflection of rays coming from peripheral facets may be enhanced by rhabdom morphology such as pointed distal tips.

Figure 20. Vectors and angles involved in calculating the extent of the blur circle on the retina of a superposition compound eye. θ, angle of incidence with the cornea, β, angle of exit from the crystalline cone layer, r, radius of curvature of the cornea, p, radius of curvature of the rhabdom layer, σ, anglular extent of the blur circle. See text for further details.

Figure 21. A flow chart depicting the ray tracing model of the *Nephrops* superposition compound eye. The model assumes parallel pencils of light enter the eye, starting with the axial facet and moving sequentially along the radius to the periphery of the aperture. The angle of incidence changes at each iteration because of the radius of curvature of the eye. URL FOR THE MODEL HERE?

Figure 22. Results from the ray tracing model of lateral and anterior regions of the eye of *Nephrops norvegicus* assuming either pointed or flat-ended rhabdoms and based on blur circle calculations from measurements of the eye in anterior and lateral areas. Figures 22 A-C show the predicted effect of varying the extent of the tapetal sheath along the rhabdom. Figures 22 D-F assume a tapetal sheath of 1/3 and show the predicted effect of varying the extent of a shielding pigment sheath along the rhabdom.

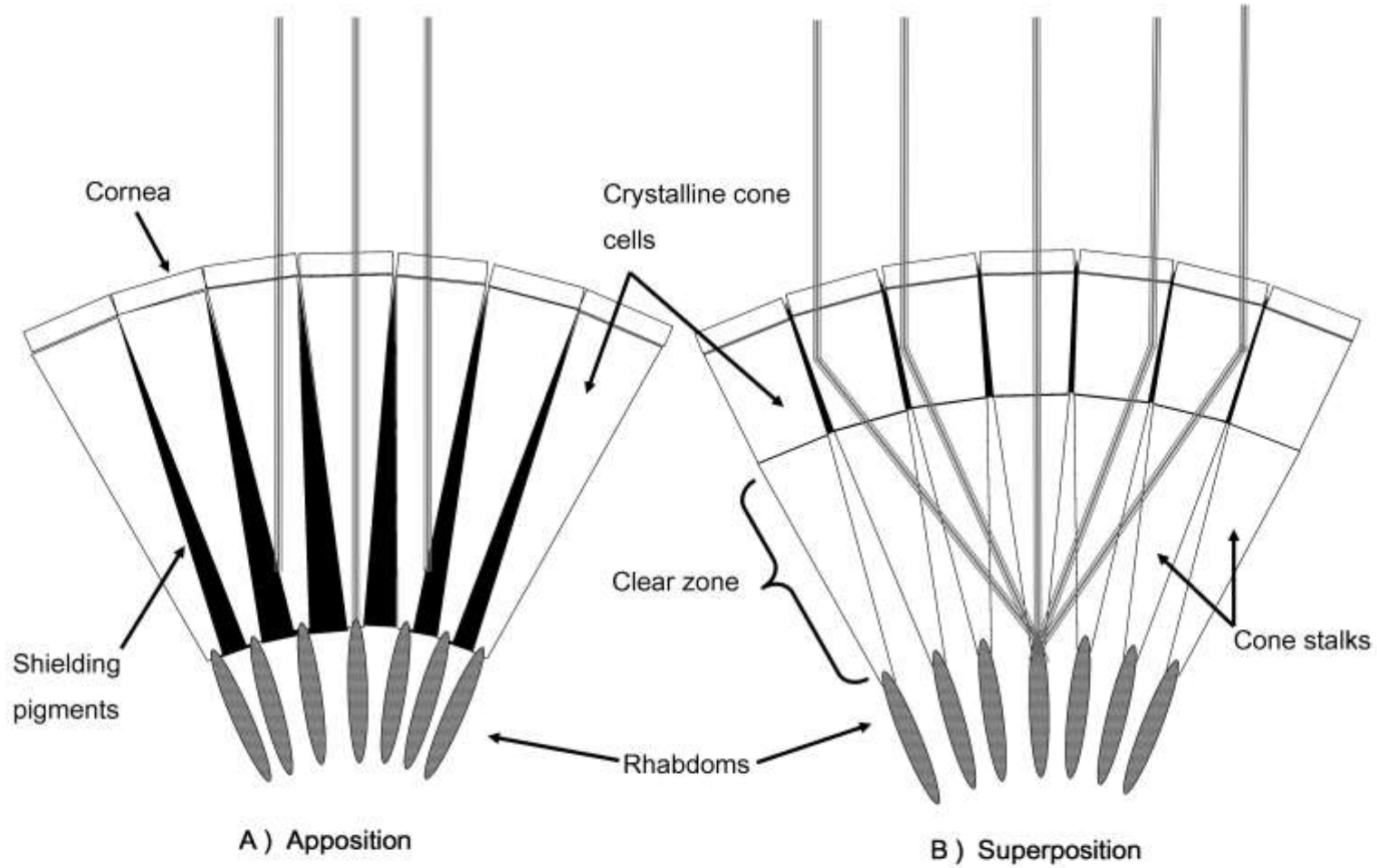
Cornea
Crystalline cone cells
Clear zone
Shielding pigments
Rhabdoms
Cone stalks
A) Apposition
B) Superposition

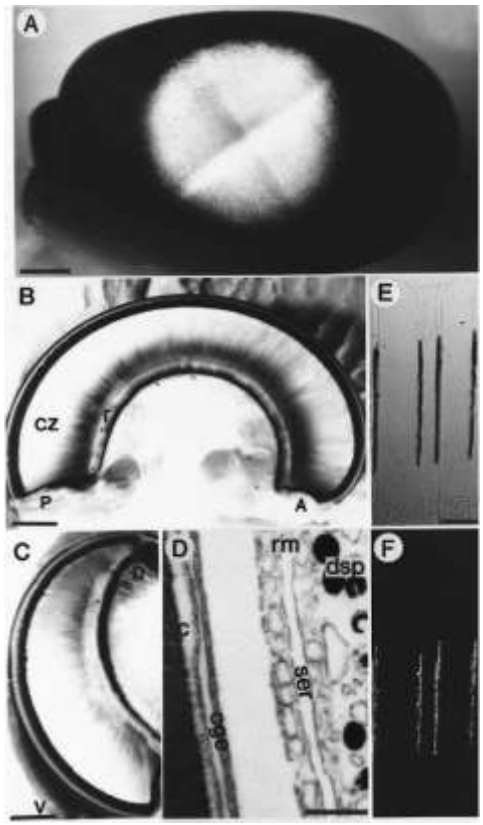
A
B
cz
P
A
E
C
D
rm
dsp
ser
cge
v
F

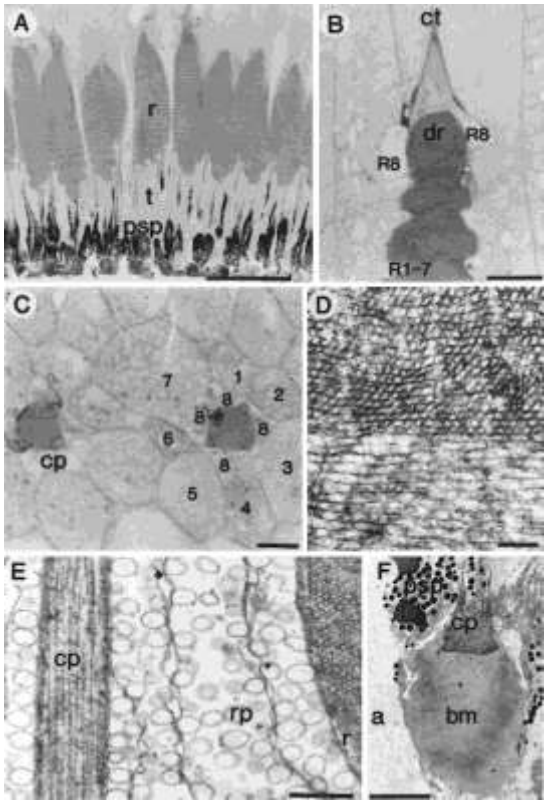
A
r
t
psp
B
ct
dr
R8
R8
R1-7
C
cp
1
2
3
4
5
6
7
8
D
E
cp
rp
r
F
psp
cp
a
bm

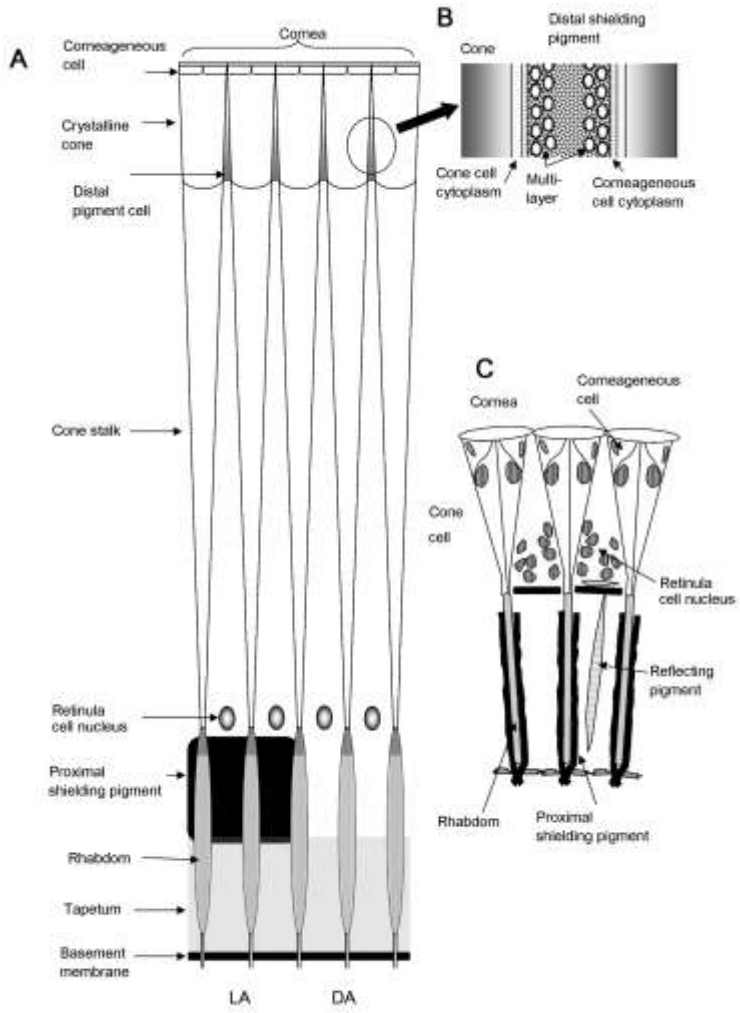
A
Cornea
Corneageneous cell
Crystaline cone
Distal pigment cell
Cone stalk
Retinula cell nucleus
Proximal shielding pigment
Rhabdom
Tapetum
Basement membrane
LA
DA
B
Distal shielding pigment
Cone
Cone cell cytoplasm
Multi-layer
Corneageneous cell cytoplasm
C
Cornea
Corneageneous cell
Cone cell
Retinula cell nucleus
Reflecting pigment
Rhabdom
Proximal shielding pigment

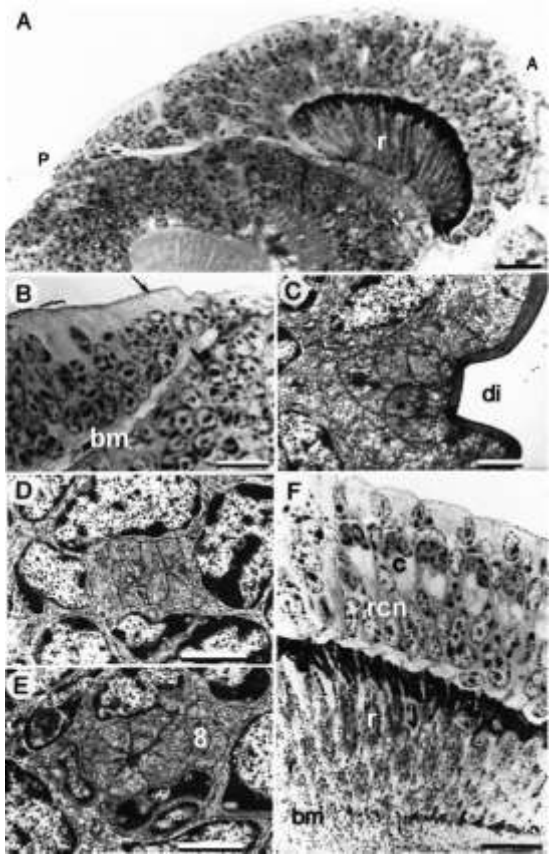
A
A
P
r
B
bm
C
di
D
F
c
rcn
E
8
r
bm

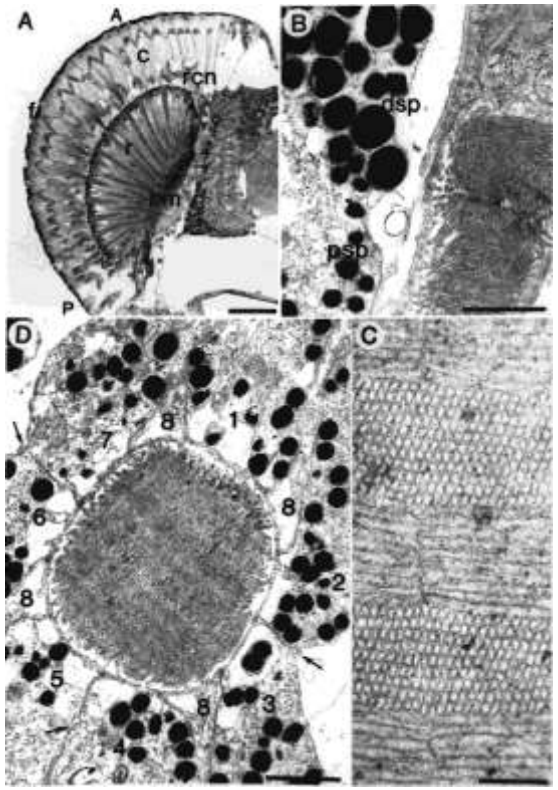
A
A
c
fcn
f
r
rm
P
B
dsp
psp
D
C
1
2
3
4
5
6
7
8
8
8
8

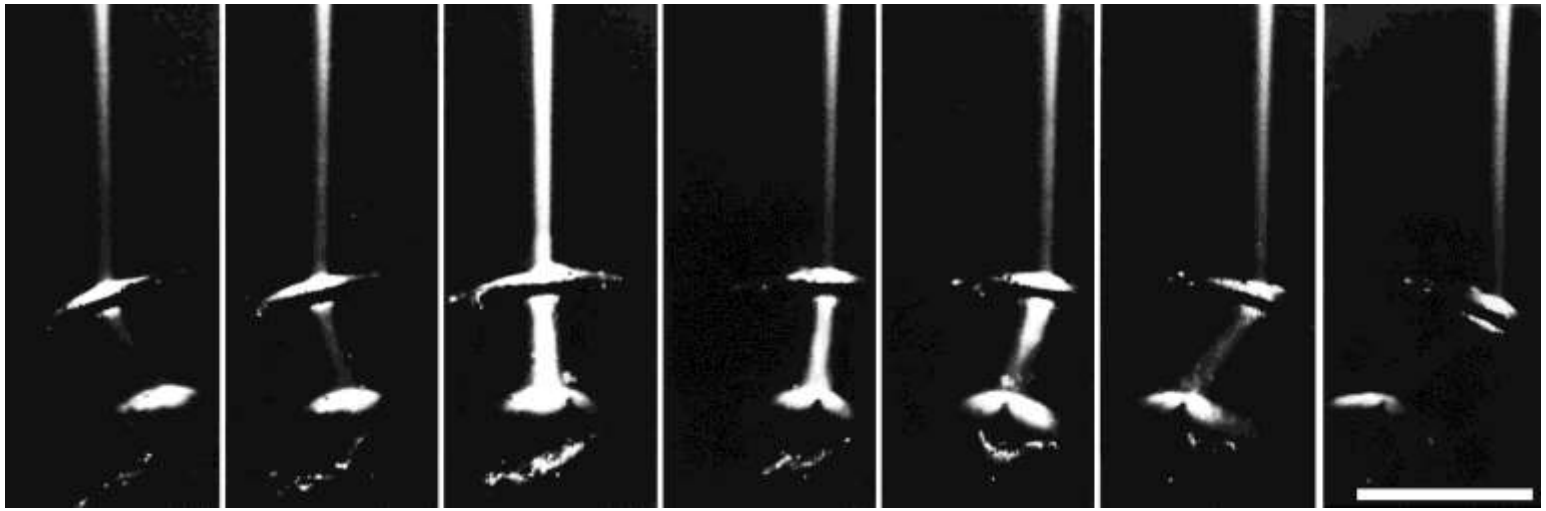

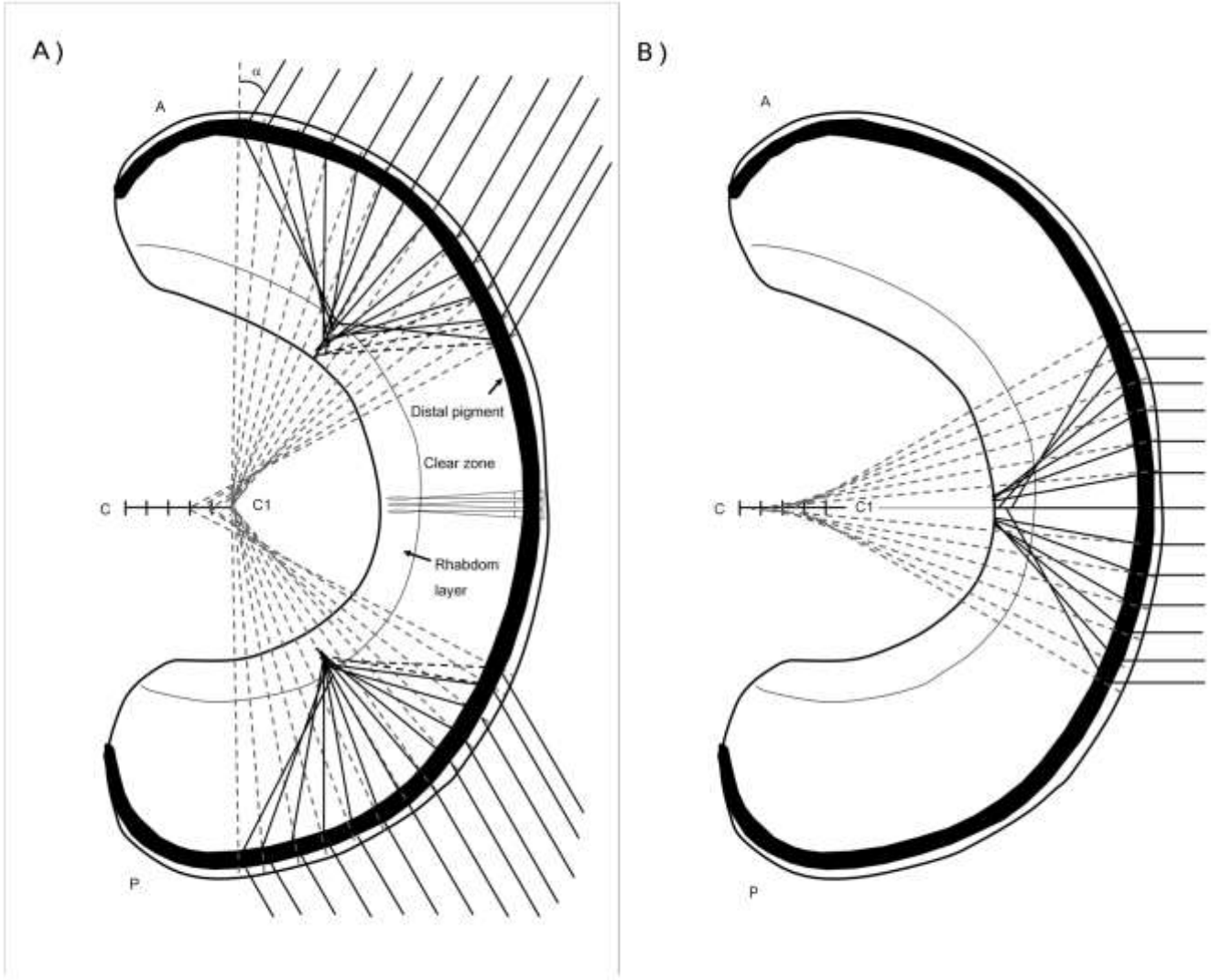
A)
α
A
Distal pigment
Clear zone
C
C1
Rhabdom
layer
P
B)
A
C
C1
P

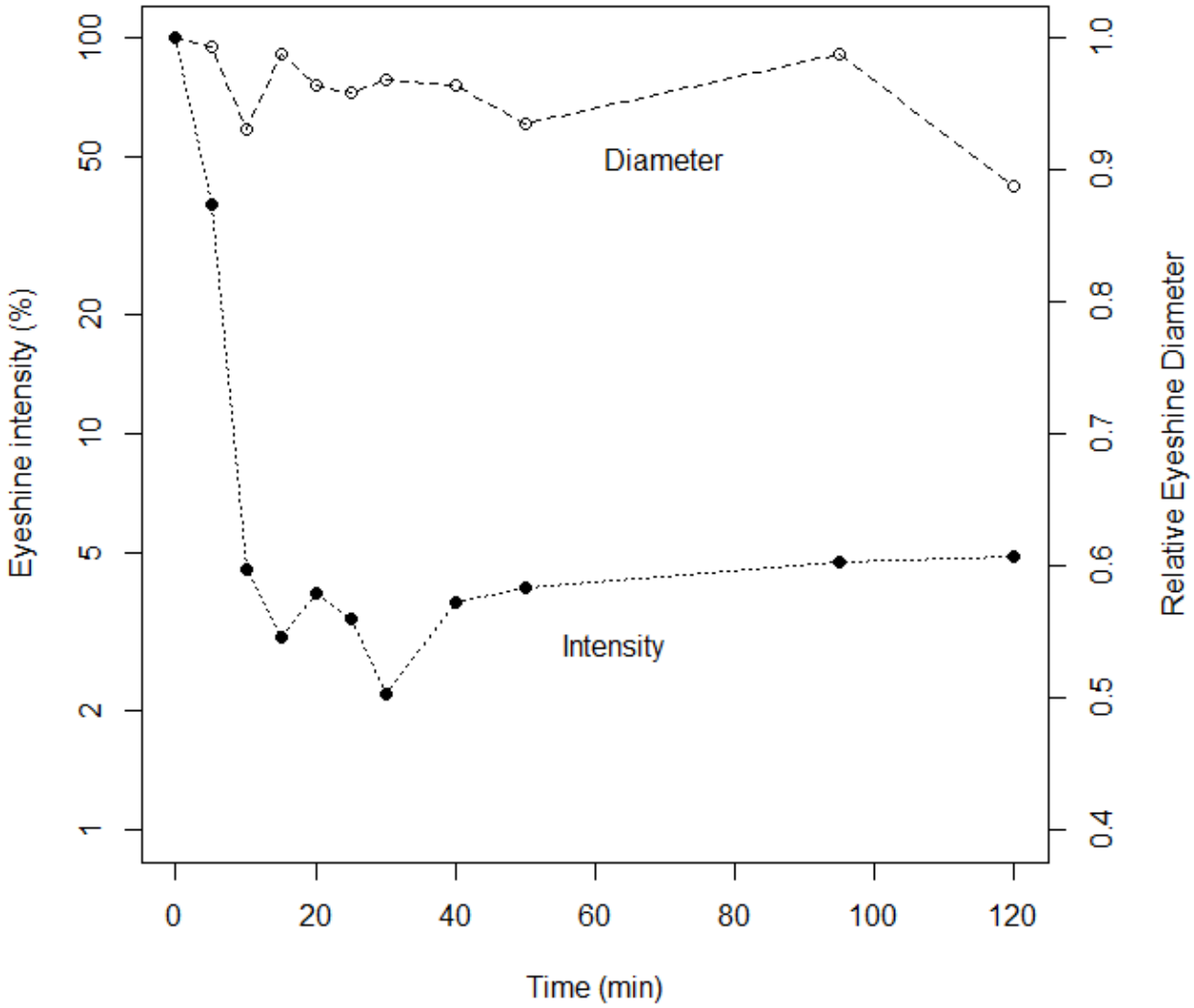
Eyeshine intensity (%)
100
50
20
10
5
2
1
Relative Eyeshine Diameter
1.0
0.9
0.8
0.7
0.6
0.5
0.4
Diameter
Intensity
0
20
40
60
80
100
120
Time (min)

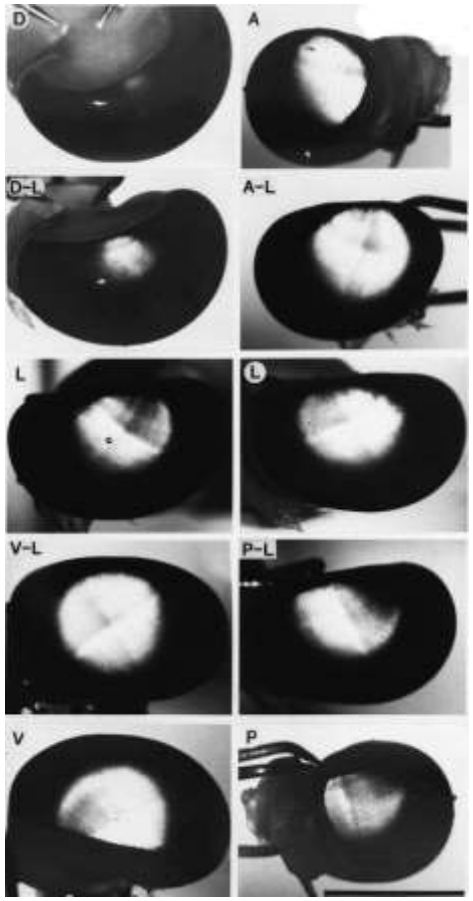
D
A
D-L
A-L
L
L
V-L
P-L
V
P

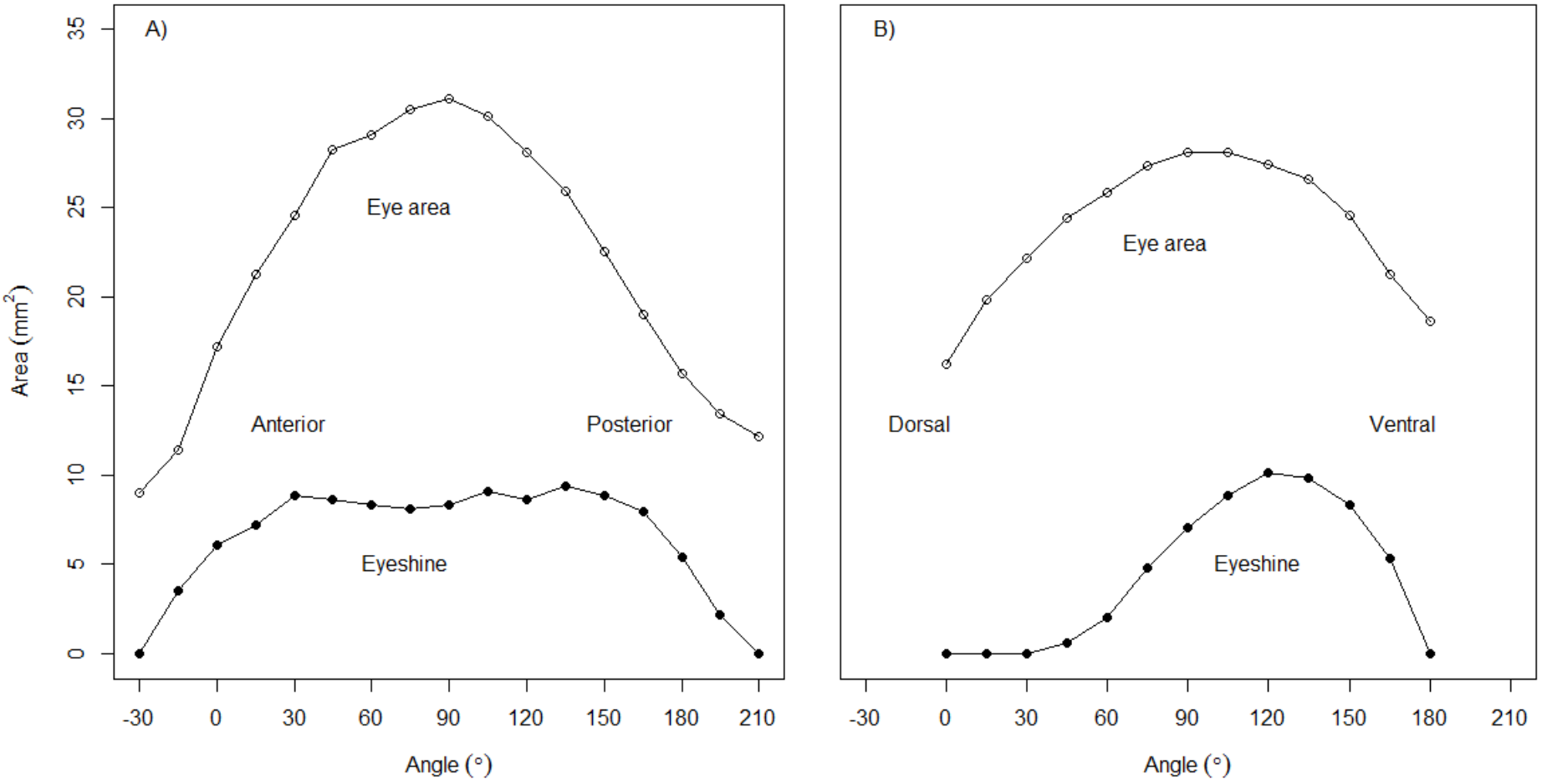
A)
Area (mm^2)
0
5
10
15
20
25
30
35
Eye area
Anterior
Posterior
Eyeshine
-30
0
30
60
90
120
150
180
210
Angle (°)
B)
Eye area
Dorsal
Ventral
Eyeshine
-30
0
30
60
90
120
150
180
210
Angle (°)

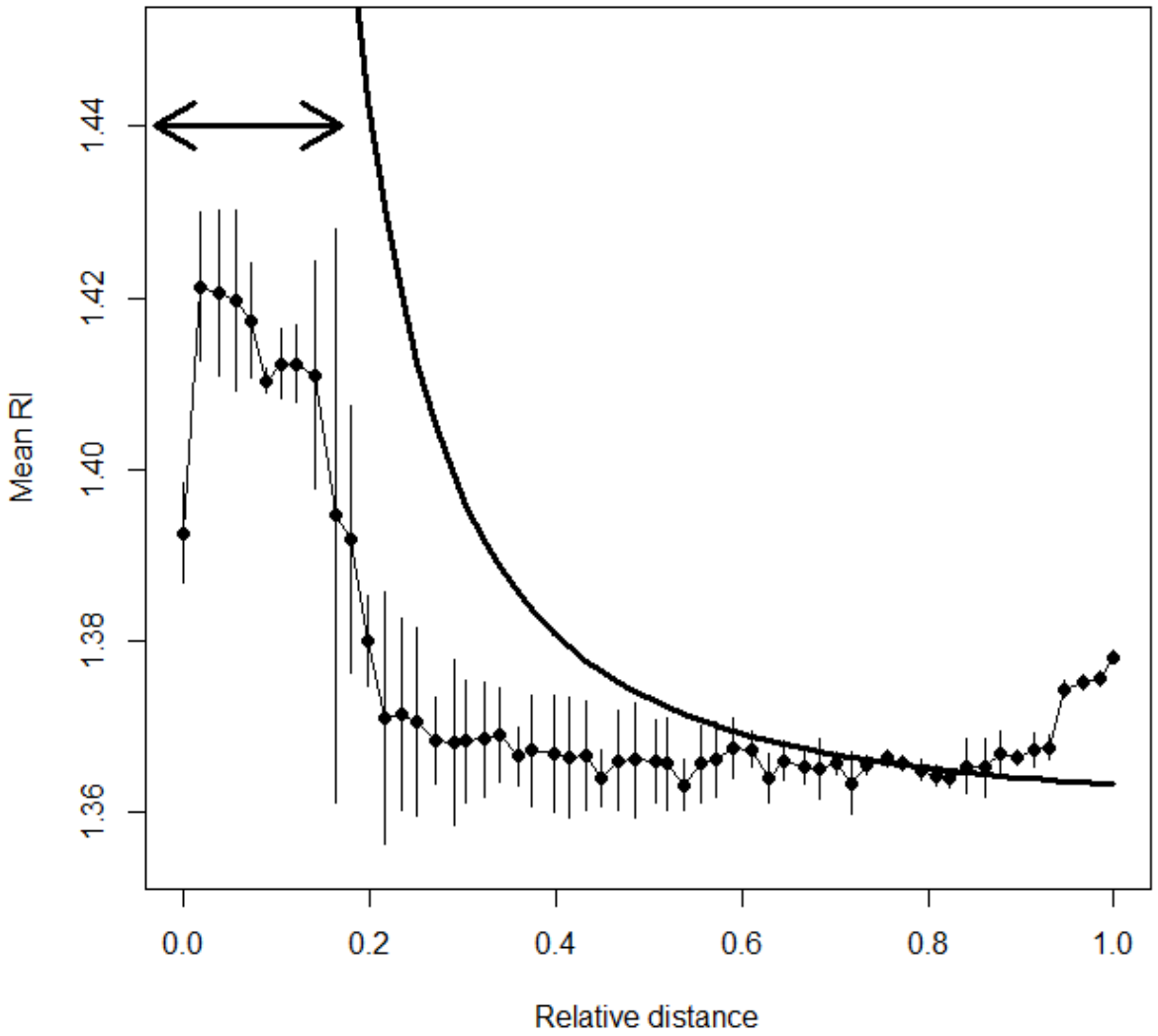
Mean RI
1.36
1.38
1.40
1.42
1.44
0.0
0.2
0.4
0.6
0.8
1.0
Relative distance

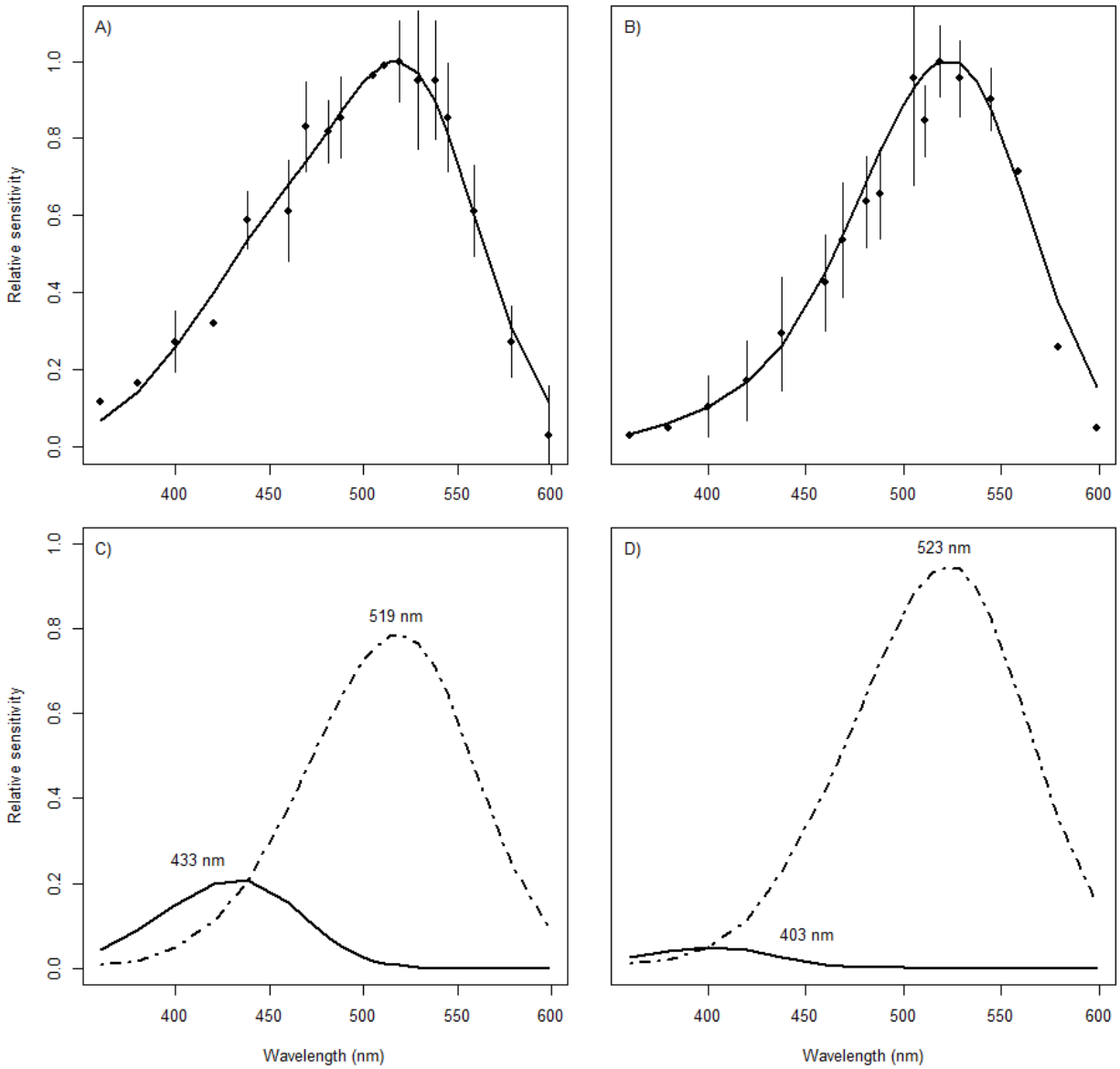
A)
B)
C)
D)
Relative sensitivity
Wavelength (nm)
519 nm
433 nm
523 nm
403 nm
0.0
0.2
0.4
0.6
0.8
1.0
400
450
500
550
600

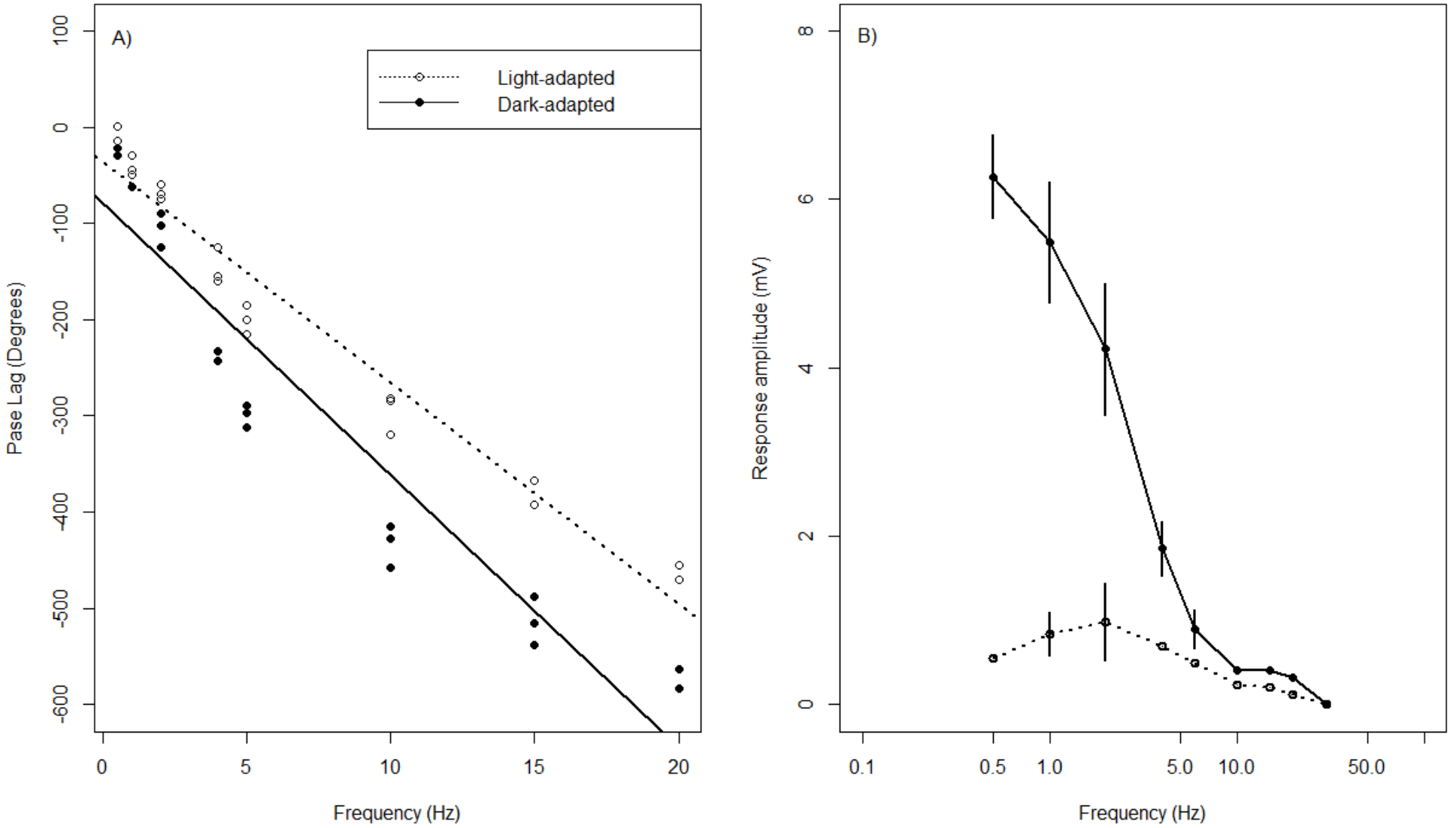
A)
Light-adapted
Dark-adapted
Pase Lag (Degrees)
100
0
-100
-200
-300
-400
-500
-600
0
5
10
15
20
Frequency (Hz)
B)
Response amplitude (mV)
8
6
4
2
0
0.1
0.5
1.0
5.0
10.0
50.0
Frequency (Hz)

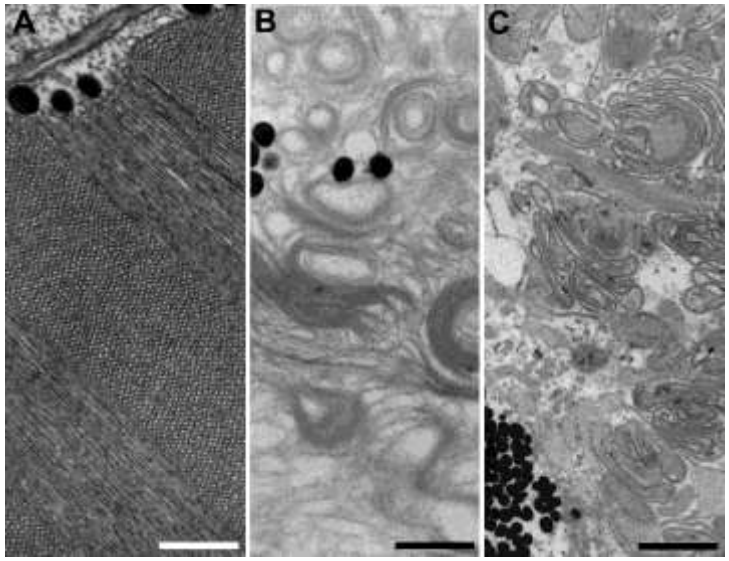
A
B
C

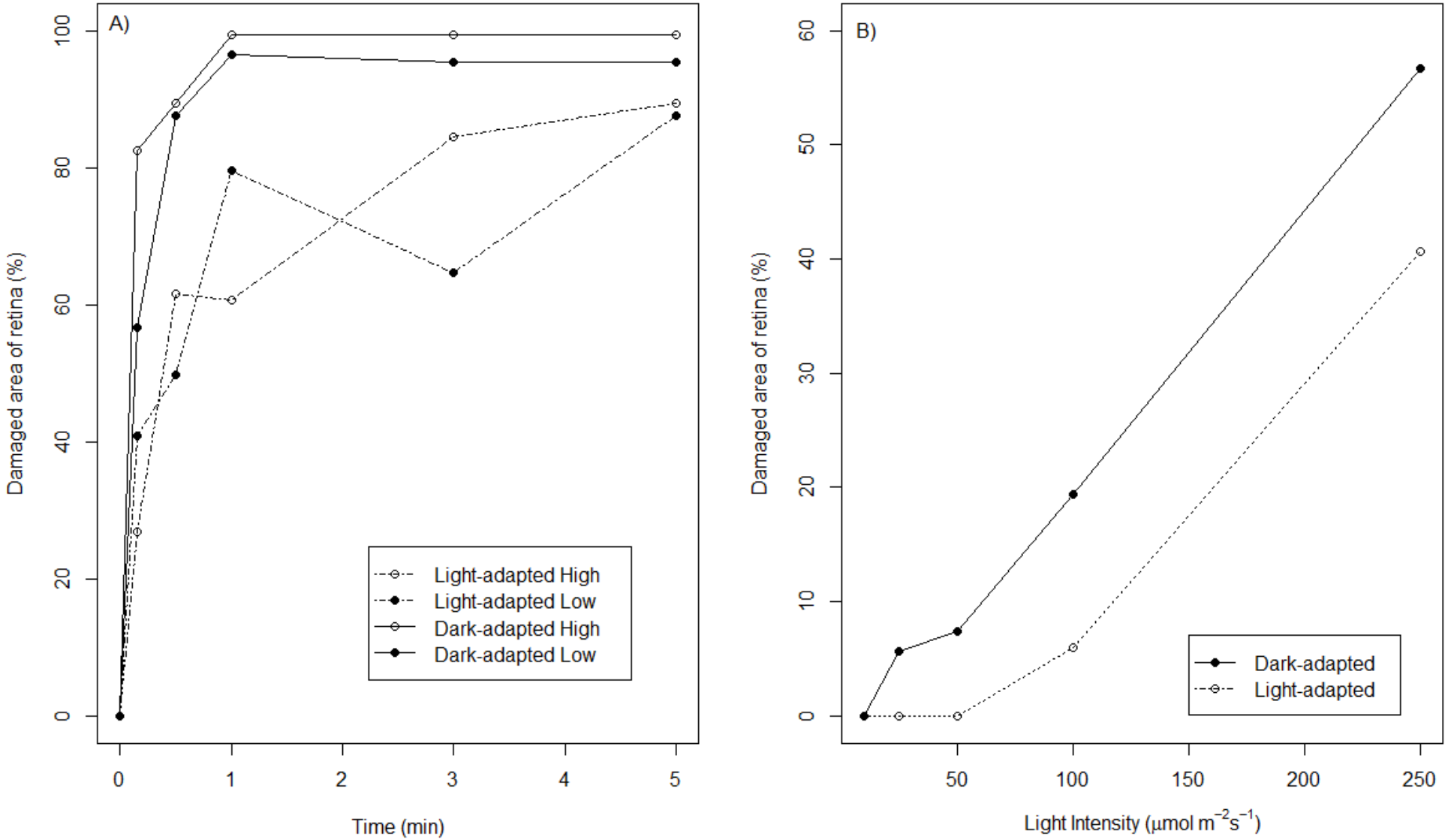
A)
Damaged area of retina (%)
0
20
40
60
80
100
0
1
2
3
4
5
Time (min)
Light-adapted High
Light-adapted Low
Dark-adapted High
Dark-adapted Low
B)
Damaged area of retina (%)
0
10
20
30
40
50
60
50
100
150
200
250
Light Intensity (µmol m^{-2}s^{-1})
Dark-adapted
Light-adapted

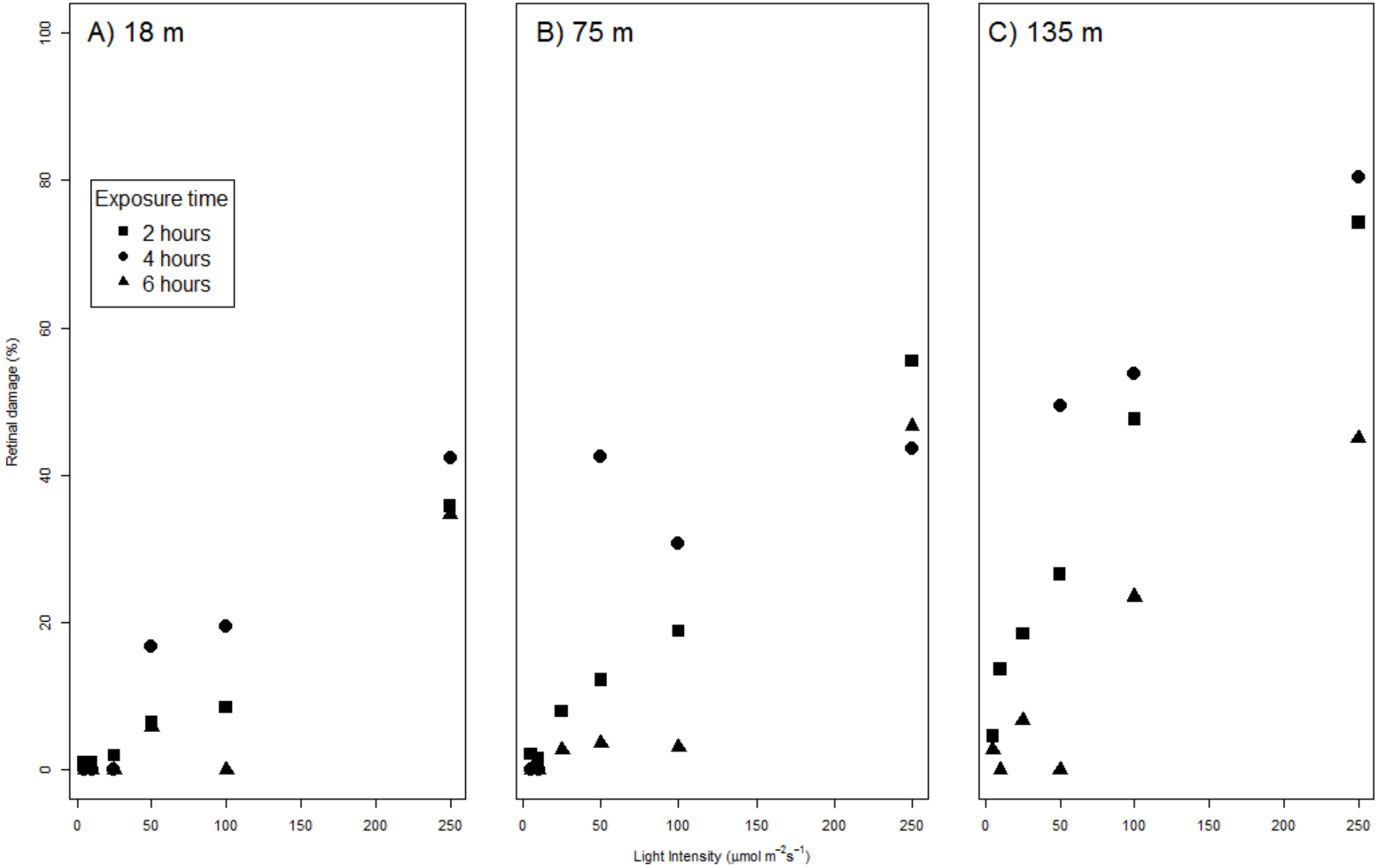
A) 18 m
B) 75 m
C) 135 m
Exposure time
2 hours
4 hours
6 hours
Retinal damage (%)
Light Intensity (µmol m^{-2}s^{-1})
0
20
40
60
80
100
0
50
100
150
200
250

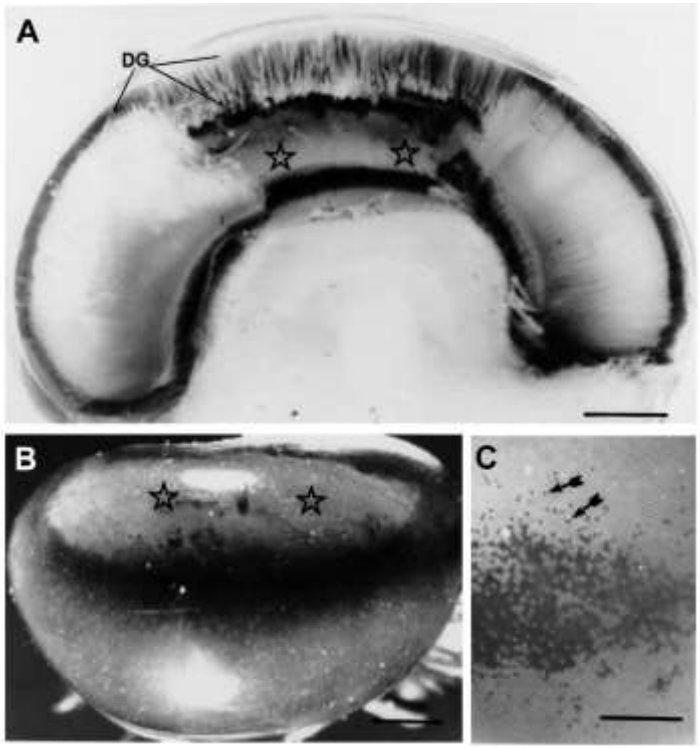
A
DG
B
C

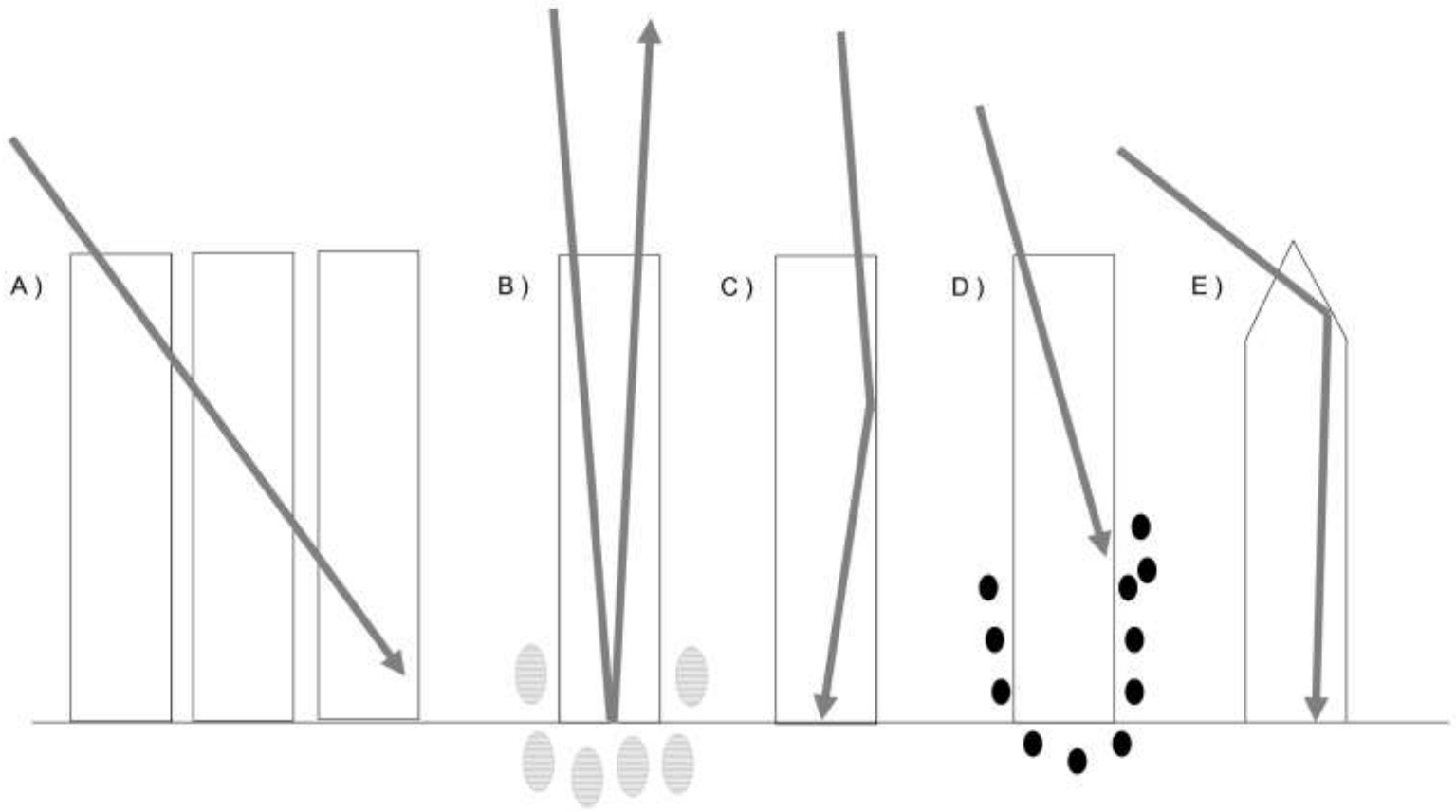
A)
B)
C)
D)
E)

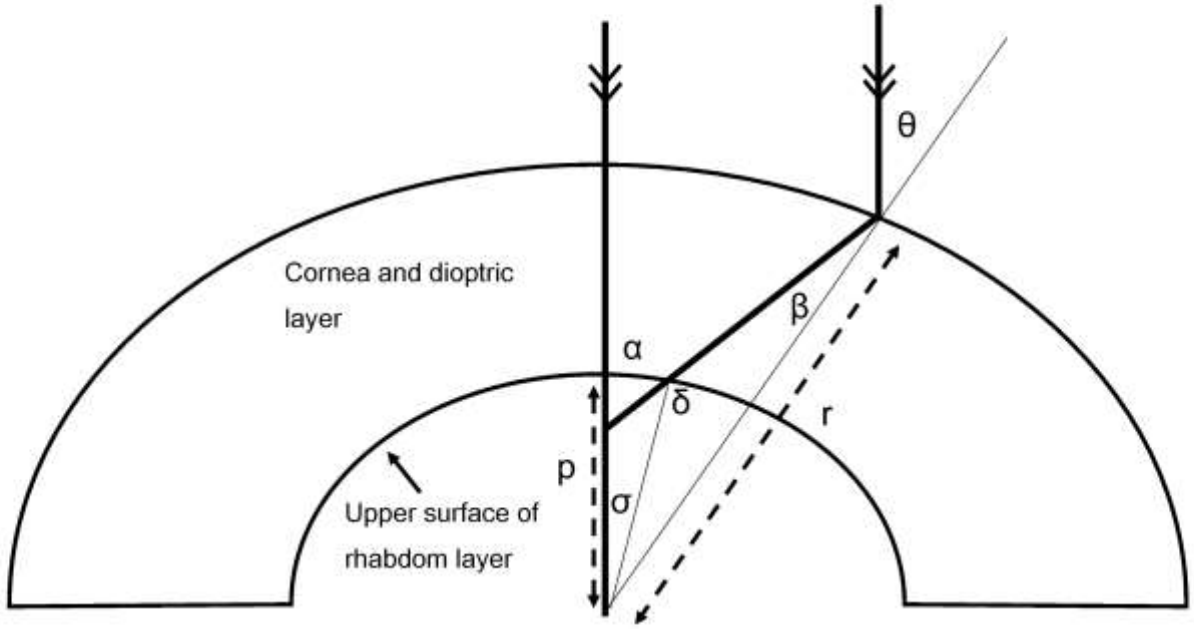
θ
Cornea and dioptric
layer
α
β
δ
r
p
σ
Upper surface of
rhabdom layer

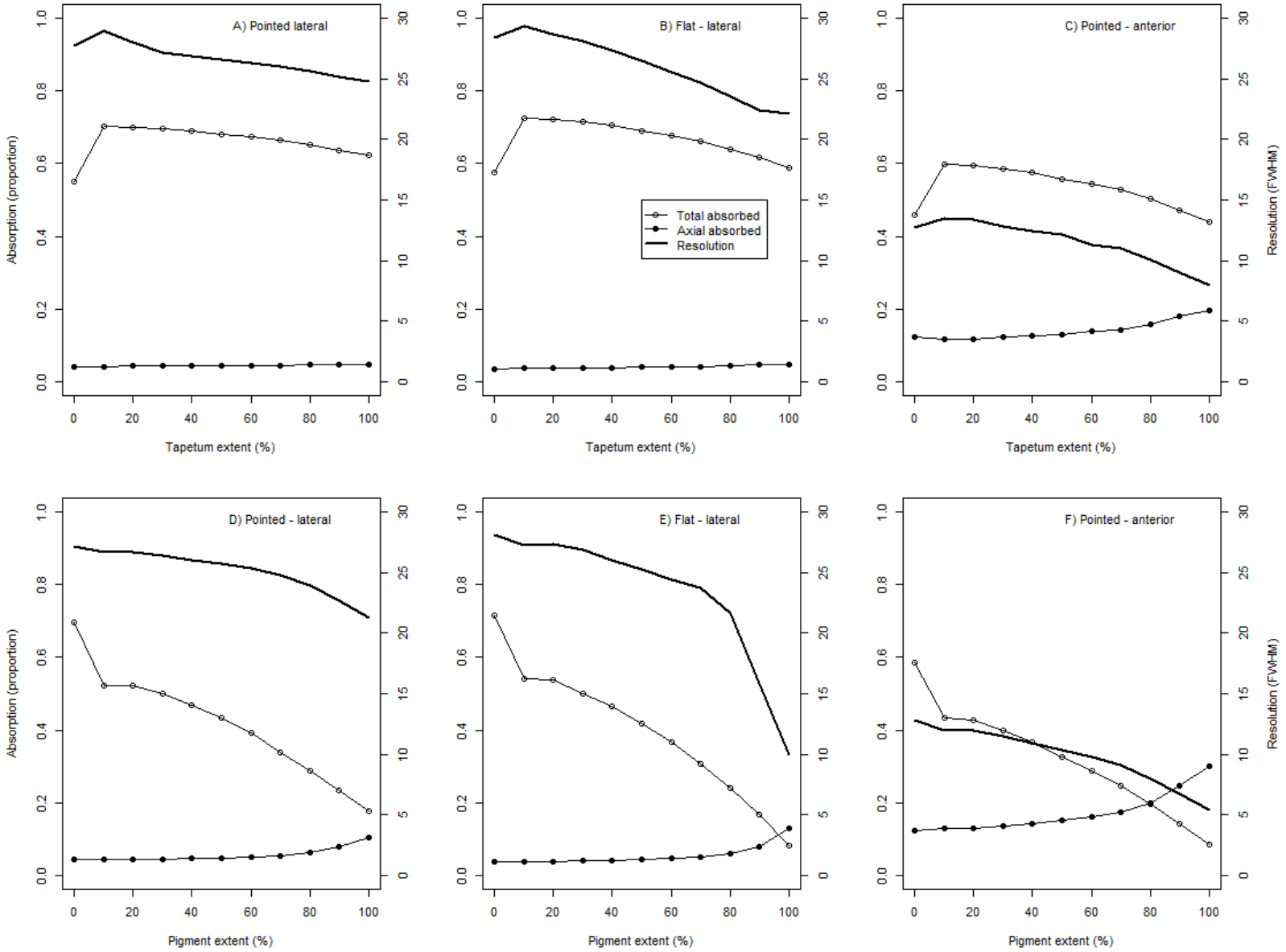
A) Pointed lateral
B) Flat - lateral
C) Pointed - anterior
D) Pointed - lateral
E) Flat - lateral
F) Pointed - anterior
Total absorbed
Axial absorbed
Resolution
Absorption (proportion)
Resolution (FWHM)
Tapetum extent (%)
Pigment extent (%)
0.0
0.2
0.4
0.6
0.8
1.0
0
5
10
15
20
25
30
0
20
40
60
80
100

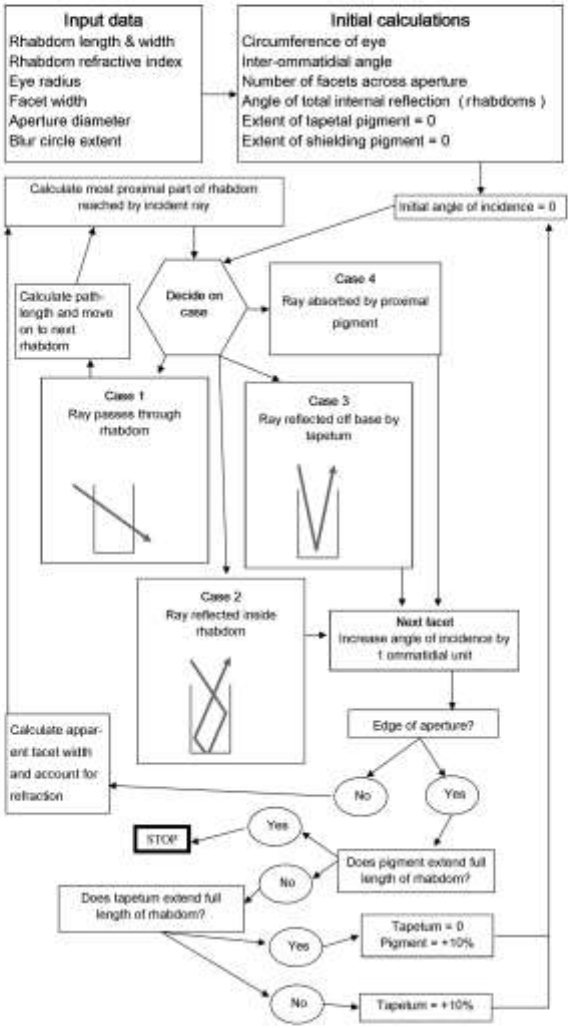
Input data
Rhabdom length & width
Rhabdom refractive index
Eye radius
Facet width
Aperture diameter
Blur circle extent
Initial calculations
Circumference of eye
Inter-ommatidial angle
Number of facets across aperture
Angle of total internal reflection (rhabdoms)
Extent of tapetal pigment = 0
Extent of shielding pigment = 0
Calculate most proximal part of rhabdom reached by incident ray
Initial angle of incidence = 0
Calculate path-length and move on to next rhabdom
Decide on case
Case 4
Ray absorbed by proximal pigment
Case 1
Ray passes through rhabdom
Case 3
Ray reflected off base by tapetum
Case 2
Ray reflected inside rhabdom
Next facet
Increase angle of incidence by 1 ommatidial unit
Edge of aperture?
Calculate apparent facet width and account for refraction
No
Yes
Yes
STOP
Does pigment extend full length of rhabdom?
No
Does tapetum extend full length of rhabdom?
Yes
Tapetum = 0
Pigment = +10%
No
Tapetum = +10%